Chapter - 5

Gas Transport Through a Blend of Glassy and Rubbery Polymer Nanocomposites

Chapter

5.1

CO_2 Separation Through Different Blends and Blend Composites Membranes

Contents

Chapter – 5.1

CO_2 Separation Through Different Blends and Blend Composites Membranes

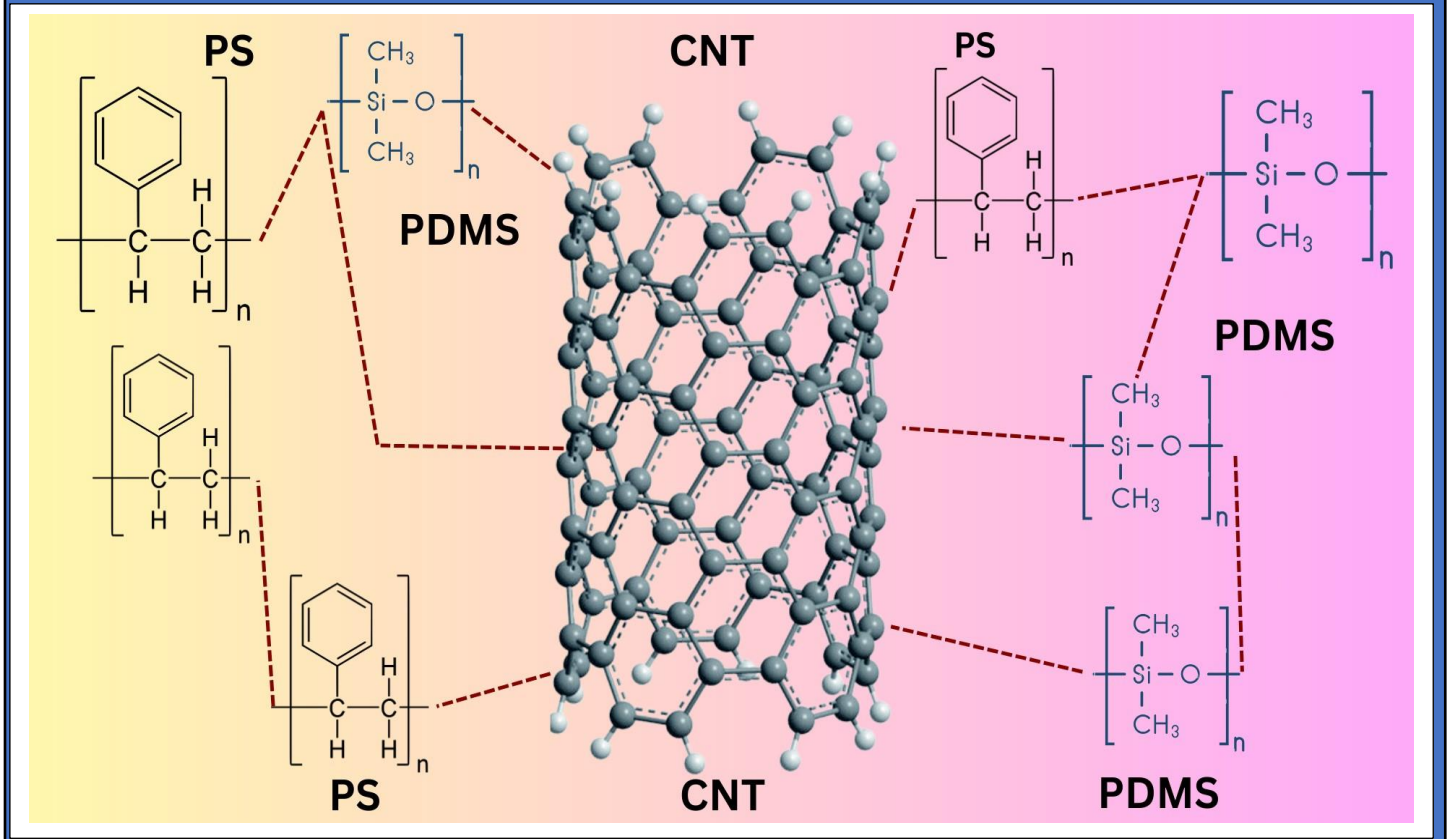

In recent scenario, polymer membranes are extensively used for gas separation, however, their efficiency is limited by the upper bound trade-off given by Robeson's in 1991 and in 2008. Some attractive modifications such as blend and composite materials have improved the performance of the membranes. More than a 90 % membrane-based business include separation of non-condensable gases like: CO_2 from CH_4, N_2 from air, H_2 from N_2 and Ar as well as from CH_4. However, some hybridisations and modifications have crossed this boundary, but further research is carried forward in this direction. It is reported that the combination of glassy and rubbery composition for gas transport process has been analysed by using blend of polystyrene (PS) and polydimethylsiloxane (PDMS). However, to make further modification the blends has been filled with CNT nanofillers to fabricate blend composite membranes and analyses by solubility, diffusivity, permeability and selectivity. The structured membrane properties of PS/PDMS - CNT have been characterized by gas permeability system, and other characterization tools. The involvement of CNTs into the blend phase improves diffusion coefficient, which in turn gains the penetrant permeability and selectivity in a tremendous manner.

5.1.1 Introduction

Mixed matrix membrane (MMM), exhibits the good combination of increasing permeability along with increasing selectivity. Glassy polymer polystyrene (PS) and a rubbery polymer polydimethylsiloxane (PDMS) have been selected as the base polymers to develop membranes for gas separation in this chapter 5.1 [1]. There are studies where PS was further stabilized by a crosslinking procedure, which improves selectivity while reducing membrane permeability when compared to controlled PDMS membranes. One of the most suitable alternatives that have been used frequently for air separation applications is polydimethylsiloxane (PDMS) [2]. In this chapter, the overcharging goal leads to develop hybrid membranes, which can improve transport parameters without loss in the trade-off separation factor. Therefore, the blending of PS and PDMS has been accomplished by a simple phase-inversion technique in our laboratory using various blending ratio such as PS/PDMS with respect to weight percentage (wt%) of PS and PDMS. An example of a blend with good miscibility and intermolecular interaction is PDMS and PS, as suggested in literature. On the mechanical and thermal characteristics of PDMS/PS blends, it is important to look into the impact of mixing PDMS and PS at various concentrations. The most recent evolution in innovative nanostructured material development is the application of nanocomposites. Moreover, the stuffing of nanoparticles into a polymer matrix may tune the properties of final

fabricated product. Despite the fact that carbon nanotubes (CNTs) are impermeable to gas molecules, embedding tiny holes enables extremely selective membrane separation of aqueous ions, liquid water, and gases [4]. Recent research indicates two-dimensional nano-porous CNT and graphene like materials that can be synthesised experimentally and are useful for CO_2 separations in industrial applications. For instance, porous CNT has been suggested for effective separation of CO_2 from CH_4, O_2, H_2 and N_2. Regardless of the manufacturing conditions, this CNT nanofillers shows inherent micro porosity results in increased fractional free volume (FFV), which leads to a very high gas permeability. Polymer nanocomposites (PNCs) are solution-processable, in contrast to the majority of other porous organic polymers. In order to obtain the requisite membrane characteristics for gas separation, by using a novel family of solvents called deep eutectic solvent (DES) to functionalize CNT nanosheets and partly replace the oxygen functional groups with hydrophilic groups. The main objective of current research is to increase the performance of CO_2 permeability, which has been often determined by the trade-off relationship. For instance, depending on the product gas specification, dehydration may be achieved using glassy and rubbery polymer blend of PS/PDMS composites with CNT nanofillers [5]. This chapter discusses the advantages of membrane-based carbon capture, including CO_2/N_2 separation in post-combustion carbon capture, CO_2/H_2 separation in syngas processing, and CO_2/CH_4 separation in natural gas sweetening. This novel strategy significantly advances sustainable energy technology by providing efficient and affordable CO_2 gas separation. Including reactive sites to aid CO_2 movement is one way to get around the Robeson's upper limit. Based on the unique chemistry of the CO_2 carrier, the studied assisted transport membranes are also discussed.

5.1.2 Experimental Set-Up

5.1.2.1 Membrane Synthesis and Characterization

Different wt% of PS and PDMS (95:5, 90:10, 87:13, 85:15, 82:18, 80:20, 78:22, 75:25, w/w%) polymers were dissolved in Dichloromethane for solution casting method. The blend of polymers with different weight ratios were mixed using a magnetic stirrer. After, the entire mixture was stirred again for 24 hr at room temperature. CNT nanofillers was separately stirred for 12 hr in a Dichloromethane, and then the mixture of PS/PDMS blend composite with different weight percentage ratios of CNT (1 wt%, 5 wt%, 10 wt% and 15 wt%) fillers was sonicated for 1 hr using probe-sonicator to avoid agglomeration and mixed the solutions again for 24 hr stirring at ambient temperature to achieve homogeneous dispersion.

This dispersed solution was put in a flask and stirred for 2 hr at 80 ± 0.1°C. After filtering, the mixture underwent multiple washings with distilled water and 50 ml of ethanol each time. This DES/CNT nanocomposite was dried for 24 hr at 80 ± 0.5°C in a vacuum oven. The solvent with PS/PDMS- CNT (1, 5, 10 and 15 wt%) and PS/PDMS-DES/CNT (1, 5, 10 and 15 wt%) was moved to a glass with a flat bottom, and the solvent put to evaporated for overnight. The mixture was placed to a glass plate and the system solvent was let to evaporate overnight. Next day, after being taken out of the petri dish, the blend composite membranes were tested for further characterization. The uniformity thickness of membrane was verified using a digital thickness meter and it was found (75 ±1) μm. Furthermore, for analyze the different parameter of the membrane the various characterization has been discussed in chapter 2.

5.1.3 Results and Discussions

5.1.3.1 Mechanical Properties

The tensile strength, Young's modulus, elongation at break, and flexural strength of a material, tensile and flexural tests of blend and blend composites membrane were performed on a Llyord EZ 20kN tensile tester at crosshead speeds of 10 mm/min and 3 mm/min, respectively, details discrimination of the instrument has been discussed in chapter 2. Polystyrene is a glassy, brittle polymer with poor toughness and a low softening temperature of 100 °C. The microstructure can be improved by adding PDMS rubbery polymer to reduce the brittleness of polystyrene. The rubber is present as second-phase particles with a diameter of around 1 mm, which greatly improves the hardness of polystyrene [7]. The tensile strength of pure PS and blend of PS/PDMS blends in various ratios are shown in Figure 5.1.1 (I and II). Figure 5.1.1 (I) shows the elongation at the break of PS and PS/PDMS blends. Figure 5.1.1 (I), $PS_{75}/PDMS_{25}$ has the longest elongation among all PS/PDMS blends and pure PS. Because of its advantages over other polymers, or because it is simple to produce using extrusion, injection, and vacuum forming, this kind of polymer is used. It has been observed that the blend elongation increases as the PDMS content increases, with the $PS_{75}/PDMS_{25}$ blends having the greatest PDMS content of all the blends. This shows how the PDMS content significantly affects the ability to extend [8]. Additionally, high elongation at break indicates a significant area below the strain-stress curve.

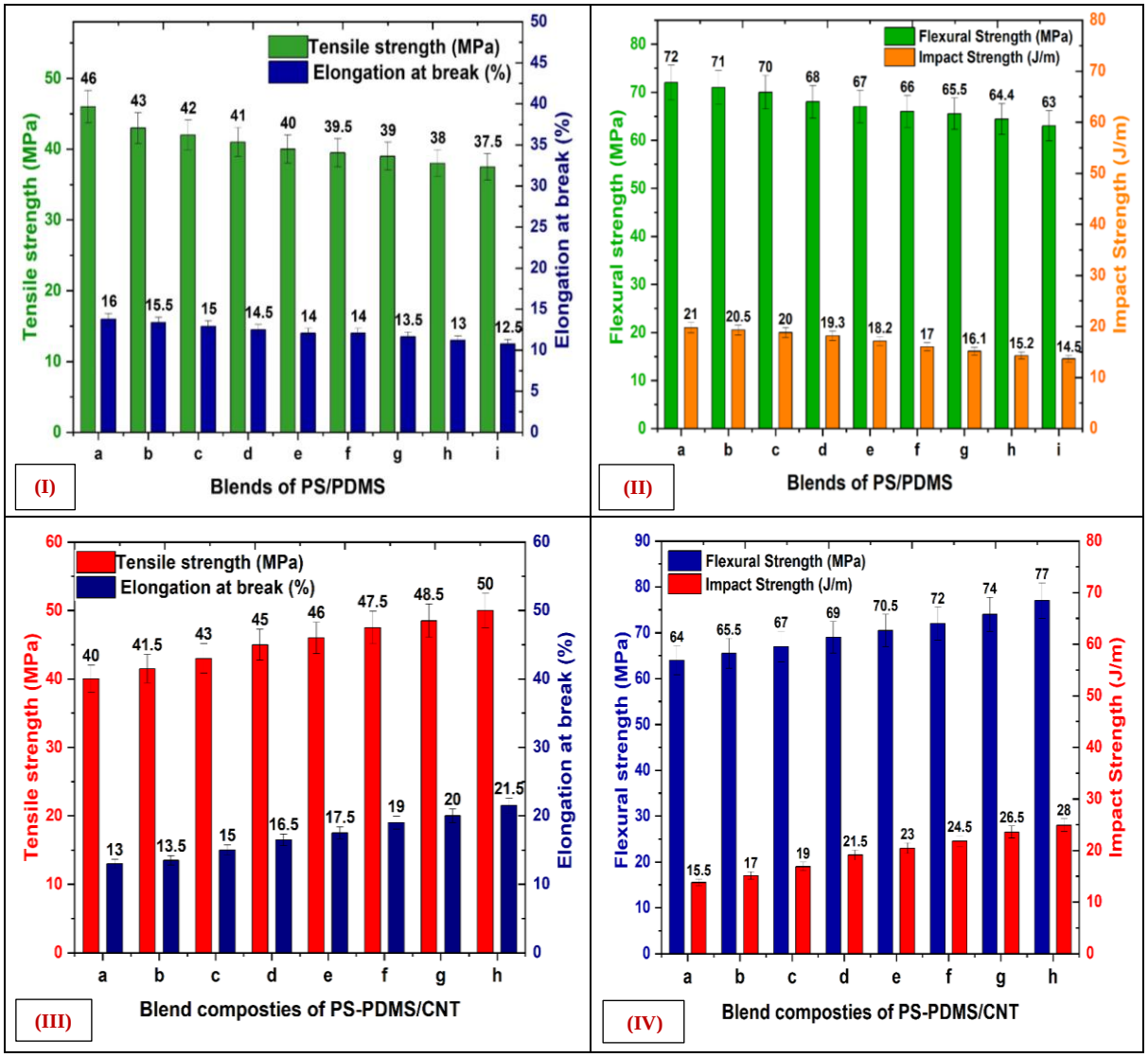

Figure 5.1.1: (I) Tensile strength and Elongation at break and **(II)** Flexural strength and Impact strength of PS/PDMS polymer blends, (a) $PS_{75}/PDMS_{25}$, (b) $PS_{78}/PDMS_{22}$, (c) $PS_{80}/PDMS_{20}$, (d) $PS_{82}/PDMS_{18}$, (e) $PS_{85}/PDMS_{15}$, (f) $PS_{87}/PDMS_{13}$, (g) $PS_{90}/PDMS_{10}$, (h) $PS_{95}/PDMS_{5}$, **(III)** Tensile strength and Elongation at break, and **(IV)** Flexural strength and Impact strength of (a) $PS_{75}/PDMS_{25}$ + 1 wt% of CNT, (b) $PS_{75}/PDMS_{25}$ + 5 wt% of CNT, (c) $PS_{75}/PDMS_{25}$ + 10 wt% of CNT, (d) $PS_{75}/PDMS_{25}$ + 15 wt% of CNT (e) $PS_{75}/PDMS_{25}$ + 1 wt% of DES/CNT (f) $PS_{75}/PDMS_{25}$ + 5 wt% of DES/CNT, (g) $PS_{75}/PDMS_{25}$ + 10 wt% of DES/CNT, (h) $PS_{75}/PDMS_{25}$ + 15 wt% of DES/CNT

This suggests that the $PS_{75}/PDMS_{25}$ blend can absorb a lot of energy, and as a result, PS/PDMS blends are expected to have high impact strength. The phenylene ring is present on every other carbon atom of PS main chain, producing a stiff, bulky shape with enough steric hindrance to make the polymer blends very rigid. The results discussed above has related to the nature of polystyrene microstructure. In contrast to the siloxane group in PDMS that is sustained on every other carbon atom of the main chain of polystyrene, the methyl methacrylate groups on every other carbon atom of the main Si chain of PDMS provide a significant amount

of steric hindrance, which makes the polymer blend (PS : PDMS) rigid and relatively strong [9].

Figure 5.1.1 (II) shows how the flexural strength of PS and their blends of PS/PDMS followed a similar pattern to that of tensile strength. Figure 5.1.1 (II), $PS_{75}/PDMS_{25}$ has a 14% greater flexural strength than pure PS and blends of PS/PDMS. It is found that the blends, with the exception of the $PS_{75}/PDMS_{25}$ blend, have the best value when compared to the blends, and have higher flexural strengths than PS. Compared to PS/PDMS blends, $PS_{75}/PDMS_{25}$ has an impact strength that is 30% greater than pure PS. This result is consistent with elongation at break, where $PS_{75}/PDMS_{25}$ exhibits the maximum elongation among PS/PDMS blends. Since it has a high energy absorption capacity before breaking. It is also observed that the impact strength of the blends has increased with the addition of PDMS up to 25 wt% with PS polymer blend, which is the highest among the blends and 27% greater than $PS_{95}/PDMS_5$. An impact strength is an essential factor in creating a novel material is having well-balanced characteristics. The stiffness and toughness characteristics of the PS/PDMS blends are shown in Figure 5.1.1 (I and II). It is clear that although its $PS_{75}/PDMS_{25}$ blend is stiff, they are as durable as PS [10]. On the other hand, the $PS_{95}/PDMS_5$ blend offers high longevity and is similarly stiff as PS. It has been observed that the $PS_{75}/PDMS_{25}$ blends have well-balanced mechanical qualities in terms of stiffness and toughness, with a tensile strength of 43 MPa and an impact strength of 20.5 J/m. The tensile strength of the blends is lower than those of each polymer as reported in literature [11]. This has brought on by PS and PDMS's strong miscibility. Due to PDMS's ability to disperse in polymers, settle in voids and interface locations, and serve as cross-linking centers between the molecules of the polymer, the addition of PDMS to blends improves their tensile strength.

In Figure 5.1.1 (III), the maximum tensile strength difference and stress-strain diagram are shown to show the tensile characteristics of the PS/PDMS-(CNT and DES/CNT) nanocomposites blend membranes [12]. The addition of CNT and DES/CNT nanofillers in the PS/PDMS blends affects the tensile characteristics. In comparison to only blends of $PS_{75}/PDMS_{25}$-CNT polymer, the tensile strength for $PS_{75}/PDMS_{25}$ - DES/CNT nanocomposites are very good and with increasing wt% of DES/CNT, the tensile strength becomes stronger. The cross-section progressively increased with increasing wt% of DES/CNT that showed many interactions between CNT and PS/PDMS. The CNTs act as a crosslinking site to connect with the polymeric chain in the composite membrane, increasing stiffness. Figure 5.1.1 (III and IV), for the PS/PDMS-CNT membrane, the tensile strength increases from 40 MPa to 45 MPa and

for the $PS_{75}/PDMS_{25}$-DES/CNT, the tensile strength increases from 45 MPa to 50 MPa, which is greater than the blends of PS/PDMS-CNT. If the CNT and DES/CNT content increased to 1 wt% to 15 wt%, the additional CNTs blocked provides enough space for the PDMS chains to move freely, which increases the mechanical strength. Notably, the flexural strength was dramatically increased from 64 MPa to 74 MPa. The resulting PS/PDMS-CNT showed elastic performance with a fracture elongation and Young's modulus respectively, after increasing the CNT and DES/CNT content to 15 wt%. These results showed that the PS/PDMS-(CNT and DES/CNT) composite membrane produced by linking the stiff with PS/CNT nano-network template and the PDMS provided both better elastic behaviour and significant tensile strength. The free radicals produced on the CNT surface, which may form more interfacial bonds with the polymer chain-end groups, may be the cause of the improved tensile strength from 40 MPa to 50 MPa. Chain mobility has increased by this crosslinking and the tensile strength started to increase at 40 MPa due to this crosslinking of CNT nanofillers with PS/PMDS blends that provides more strength to PS/PDMS composite membranes [13]. The addition of DES/CNT nanofillers doses affect the much more mechanical strength as compared to only CNT nanofillers in PS/PDMS nanocomposite blends.

5.1.3.2 Differential Scanning Calorimetry (DSC)

Figure 5.1.2 shows the DSC thermogram of PS/PDMS blends and blend composites of PS/PDMS-CNT with different weight ratios, details of DSC instrument has been discussed in chapter 2. The glass transition (T_g) and melting temperature (T_m) are observed for all samples. It is observed that $PS_{75}/PDMS_{25}$ has a greater T_g than $PS_{95}/PDMS_5$ blends due to PDMS has more siloxane linkages than that of PS, making it more polar; as a result, more energy is required to break the interchain interactions [14]. For all PS/PDMS blends a single T_g value is seen, indicating miscibility in the amorphous region. Additionally, it is clear that the T_g value decreases as PDMS content increases as reported in literature [15]. Chain mobility was likely made possible by the creation of block copolymers as a result of the transesterification process. T_g of these three blends, were found to be nearby values, showing partial miscibility [16]. The PDMS polymer has a crystallization temperature of about 45.2 °C and is highly susceptible to crystallization. It is obvious that the addition of diphenyl groups to the polymer chain completely suppresses crystallization. On the other hand, since the PS polymer improves the stiffness of the polymer chain, the T_g of the co-polysiloxanes repeatedly increases with increasing quantities of the diphenyl group [17].

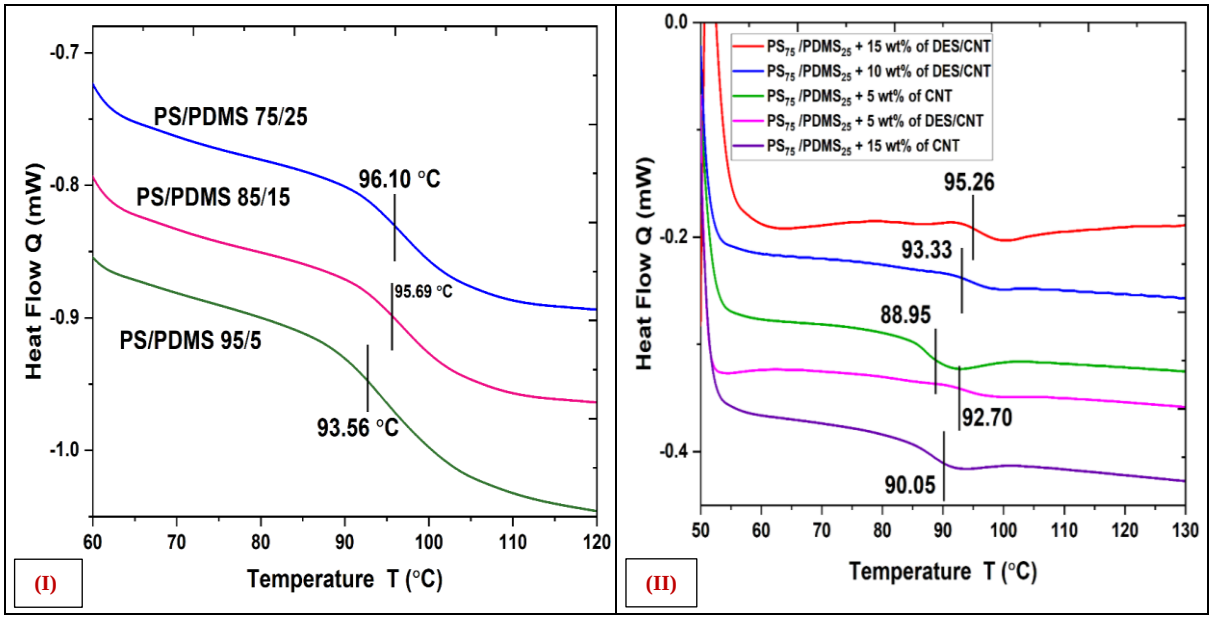

Figure 5.1.2: DSC thermogram of **(I)** PS/PDMS blends with different wt% ratios like $PS_{75}/PDMS_{25}$, $PS_{85}/PDMS_{15}$, $PS_{95}/PDMS_5$ and **(II)** thermogram of $PS_{75}/PDMS_{25}$ composites with different wt% of CNT and DES/CNT

As a result, the T_g values for co-polysiloxanes are found to be between 90 °C and 95 °C. No any T_g is seen in this temperature range above 100 °C, when the diphenyl group amounts are above than 25 wt%, as shown in Figure 5.1.2 (I). The T_g increases from 93.56 °C to 95.69 °C to 96.10 °C, respectively, while the diphenyl group PDMS concentration increased from 5 wt% to 15 wt% and 15 wt% to 25 wt% [18]. This may be explained by the fact that the PDMS unit interrupts the polysiloxane molecular structure's symmetry and regularity, which prevents crystallization. The results point to the co-polysiloxanes random nature, which is similar to those of PS/PDMS blends. The DSC results show that the co-polysiloxanes are amorphous and that the T_g increases with the amount of diphenyl siloxane in the polymer chain.

When nanofillers of CNT and DES/CNT were added, there was a noticeable change in T_g; rather, the reduction in heat capacity was ascribed to the immobilisation of the polymer at the surface of the CNT particles. It was observed that the shift in T_g after addition of CNT and DES/CNT nanofillers into the polymeric blend of PS/PDMS based on the observed patterns in the DSC curves for nanocomposite membrane. T_g can be shown to be impacted for all samples, however the sample with 15 wt% of DES/CNT nanofillers shows an unexpected behaviour, the value of T_g for $PS_{75}/PDMS_{25}$ + 15 wt% of DES/CNT is optimized 95.26 °C, as shown in Figure 5.1.2 (II). In accordance with this concentration of DES/CNT nanofillers, has a significant increase in T_g was observed. Repeated scans confirmed this behaviour, which

seems to be independent of epoxy curing. Conduction percolation has been thought to be connected to the arrangement of the conducting particles in the blend matrix. Particles arrange themselves in definite infinite patterns at the percolation threshold, but before that, they exist in finite size clusters. The result shows that adding CNT and DES/CNT into a PS/PDMS polymer blend increases free volume due to its nucleating impact [19].

5.1.3.3 Thermogravimetric Analyzer (TGA)

According to Figure 5.1.3 (I) TGA curves, Figure 5.1.3 (II) DTA curves of PS/PDMS blends in nitrogen, the addition of PDMS silica increased the thermal stability of PS/PDMS blends [20]. There is a rapid weight loss at a limited range of 390 ^{o}C – 430 ^{o}C, however the weight loss is initially slow and steady (less than 3%).

Thermal decomposition of PDMS has primarily caused by the breakdown of C=C bonds, but it also involves the breakdown of head-head bonds, hydrocarbons at the ends of polymeric chains, and random polymer chain breaking [21]. By decreasing the decomposition temperature at which PS/PDMS blend decomposes and increasing the char yield, it is clear that adding PDMS improves thermal stability even more.

The degradation temperatures were found to be in the range of 300 °C to 320 °C, 360 °C to 380 °C, from 380 °C to 410 °C, and from 390 °C to 430 °C for weight losses of 10%, 25%, 50%, and 75%, respectively, when PDMS concentration was increased from 0 to 25 wt% as shown in Figure 5.1.3 (I).

Compared to the other nanocomposite membranes, PS/PDMS blends with a higher amount of DES/CNT and CNT nanofillers has lost less weight, demonstrating that the CNT nanofillers greatly increases the heat stability of the PS/PDMS nanocomposite blend membranes, as shown in Figure 5.1.3 (III).

This phenomenon has been explained by a number of processes: (a) dispersed nanotubes can decrease the flow of degradation product; (b) Polymer chains close to nanotubes degrade more slowly; the start of degradation is delayed, and (c) better thermal conductivity in the polymer/nanotube composites allows for more heat dissipation inside the composite [22,23].

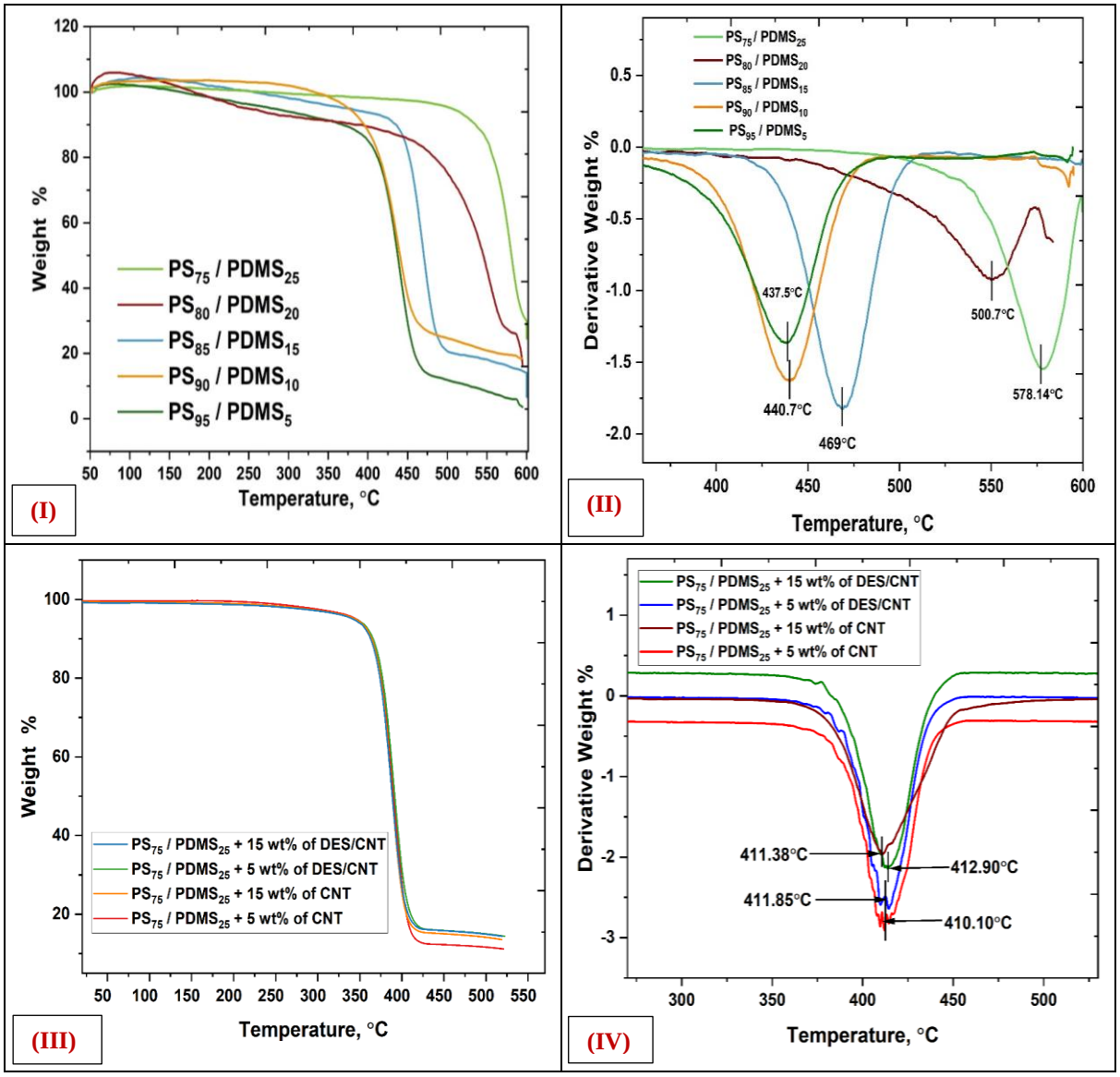

Figure 5.1.3: (I and II) TGA thermograms and DTA curves of PS/PDMS blends with different wt% ratio, $PS_{75}/PDMS_{25}$, $PS_{80}/PDMS_{20}$, $PS_{85}/PDMS_{15}$, $PS_{90}/PDMS_{10}$, $PS_{95}/PDMS_5$ and **(III and IV)** TGA thermogram and DTA curves of $PS_{75}/PDMS_{25}$ composites with different wt% of CNT and DES/CNT nanofillers

Figure 5.1.3 (III and IV), shows the thermal stability of the PS/PDMS blends nanocomposite with different wt% of CNT and DES/CNT nanofillers. It has been divided these entire mass losses of heat degradation into four main parts as shown for all samples. The presence of moisture on the sample surface is to blame for the 5% of weight loss that occurred during the first stage of the deterioration (50 °C - 380 °C) [22]. PS/PDMS-(CNT and DES/CNT) nanocomposite membranes showed a rapid weight loss of around 50% of weight loss in the second stage (380 °C – 400 °C), which is consistent with the depolymerisation of the siloxane chains [23].

Table 5.1.1: TGA analysis of polymer blends of PS/PDMS and PS/PDMS blends composites with different wt% of CNT and DES/CNT nanofillers with mass weight loss of membranes

Polymer Blends	$T_{5\%}$ (°C)	$T_{10\%}$ (°C)	$T_{50\%}$ (°C)	T_{max} (°C)	Char yield (wt%) 600 °C
$PS_{75}/PDMS_{25}$	320	370	578	615	5.5
$PS_{80}/PDMS_{20}$	318	365	500	610	4.2
$PS_{85}/PDMS_{15}$	316	360	469	600	2.5
$PS_{90}/PDMS_{10}$	310	358	440	594	1.3
$PS_{95}/PDMS_{5}$	304	356	437	588	0
$PS_{75}/PDMS_{25}$ + 15 wt% of DES/CNT	378	401	408	412	6.2
$PS_{75}/PDMS_{25}$ + 5 wt% of DES/CNT	365	397	405	411	4.5
$PS_{75}/PDMS_{25}$ + 15 wt% of CNT	355	388	403	411	3.1
$PS_{75}/PDMS_{25}$ + 5 wt% of CNT	346	379	402	410	1.9

Temperatures between 400 °C and 409 °C may be attributed to the oxidation process in the third stage and around 95% of weight loss occurred between 400 °C and 409 °C. The last step involves weight loss caused by carbon nanotube decomposition at temperatures between 409 °C and 413 °C. Table 5.1.1, shows the percentage of weight loss at different temperatures like $T_{5\%}$ (°C), $T_{10\%}$ (°C), $T_{50\%}$ (°C), $T_{max\%}$ (°C) and char yield. TGA shows that when temperatures increase, there is a gradual loss of weight that eventually amounts to 97% of the original weight in case of the polymer blends of PS/PDMS, char makes up the remaining 3%. Two phases of weight loss are shown on the thermogram of the nanocomposites in Figure 5.1.3 (III and IV). The silica in PDMS gives the polymer blend more stability at this point. According to Table 5.1.1, compared to the five different polymer blends, the addition of Si oxides increases the temperature ($T_{50\%}$) at which 50% of weight loss has happened. The proportion of weight loss is smaller in the second stage, when the polymer chain begins to

break down, where silica and carbon have a bigger impact. After heat, the proportion of char increases, which clearly shows the beneficial influence on thermal stability [22]. The results show that the amount of the addition of PDMS polymer affects the increased stability. As expected, the PDMS polymer significantly reduces the thermal decomposition of PS/PDMS blend polymer [18,22]. The PDMS filled PS/PDMS relative thermal stability was consistent with its physico-mechanical characteristics. TGA studies show that the addition of the diphenyl siloxane PDMS polymer results in increased thermal stability.

To measure the thermal stability of the membranes, maximum decomposition temperature (Td_{max}) was used. Td_{max} values have been found to be 412.90 °C, 411.85 °C, 411.38 °C, and 410.10 °C for composites membranes with 15 wt% of DES/CNT, 5 wt% of DES/CNT, 15 wt% of CNT and 5 wt% of CNT content, respectively. The char yield at 500 °C has been studied to determine the impact of CNT composites addition on the thermal stability of PS/PDMS blends. The char yield in TGA is a significant parameter that provides valuable information about the thermal decomposition behaviour of a material. Char yield represents the percentage of the original sample that remains as a solid residue after undergoing thermal decomposition. It provides a quantitative measure of the stability of a material and its ability to withstand high temperatures without completely decomposing. In the analysis of polymers, char yield is particularly relevant. It can indicate the extent to which a polymer undergoes thermal degradation and forms a solid char yield or residue. This information is crucial for understanding the thermal stability and decomposition pathways of polymers. The value of char yield (%) at 500 °C for $PS_{75}/PDMS_{25}$ + 15 wt% of DES/CNT is 6.2%, $PS_{75}/PDMS_{25}$ + 5 wt% of DES/CNT is 4.5%, $PS_{75}/PDMS_{25}$ + 15 wt% of CNT is 3.1%, $PS_{75}/PDMS_{25}$ + 5 wt% of CNT is 1.9%. As a result, the thermal stability of PS/PDMS blend membranes could certainly be improved by the suitable addition of DES/CNT and CNT nanofillers. The results show that the addition of the DES/CNT nanofillers causes nanocomposites blends of PS/PDMS to weigh much less than only blends composites of PS/PDMS-CNT. The DES/CNT composites in the current study are thermally stable up to 500 °C, and it was the greatest percentage among the other available options. The results show that the temperature of maximal thermal deterioration would increase with the addition of DES/CNT nanofillers. The increased degree of cross-linkage and crystallinity of the matrix material may be the cause of the composites improved heat stability.

5.1.3.4 Fourier Transform Infrared (FT-IR) Spectroscopy

Using FT-IR spectrometer, the infrared absorption spectra of functional groups from the blends of PS/PDMS and samples were obtained as shown in Figure 5.1.4., the details of FT-IR instrument has briefly discussed in chapter 2. A sharp and intense peak at 2900 cm^{-1} due to the vibration of the aromatic C-H Stretch group. The main PDMS absorption peaks between blends of PS/PDMS are shown not to vary significantly [23]. Different functional groups in PDMS were found to exist at wavenumbers of 2972 cm^{-1} (C-H stretching in -CH_3), 710 cm^{-1} (CH_3 symmetric bending in Si-CH_3), 1096 cm^{-1} and 1008 cm^{-1} (Si-O-Si), and at 1610 cm^{-1} (CH_3 rocking in Si-CH_3) [24]. This suggests that the main chemical interaction in PDMS is significant after blending with PS/PDMS. By increasing the strength of Si-CH_3, Si-O-Si and –CH_2 vibration when PDMS polymer has added to the PS/PDMS polymer blend, it is possible to draw the conclusion that the functional groups of PDMS play a role in the interaction between the two components [11,25]. The vibration caused by the stretching of the -Si group in ester bonds is responsible for the broad peak between 1600 cm^{-1},1000 cm^{-1} and 700 cm^{-1}. Due to the bending and stretching of C-H, there is a sharp band with medium intensity between 650 cm^{-1} and 500 cm^{-1} and a broad band with reduced intensity between 3200 cm^{-1} and 2900 cm^{-1}, as observed in Figure 5.1.4 (I) [25].

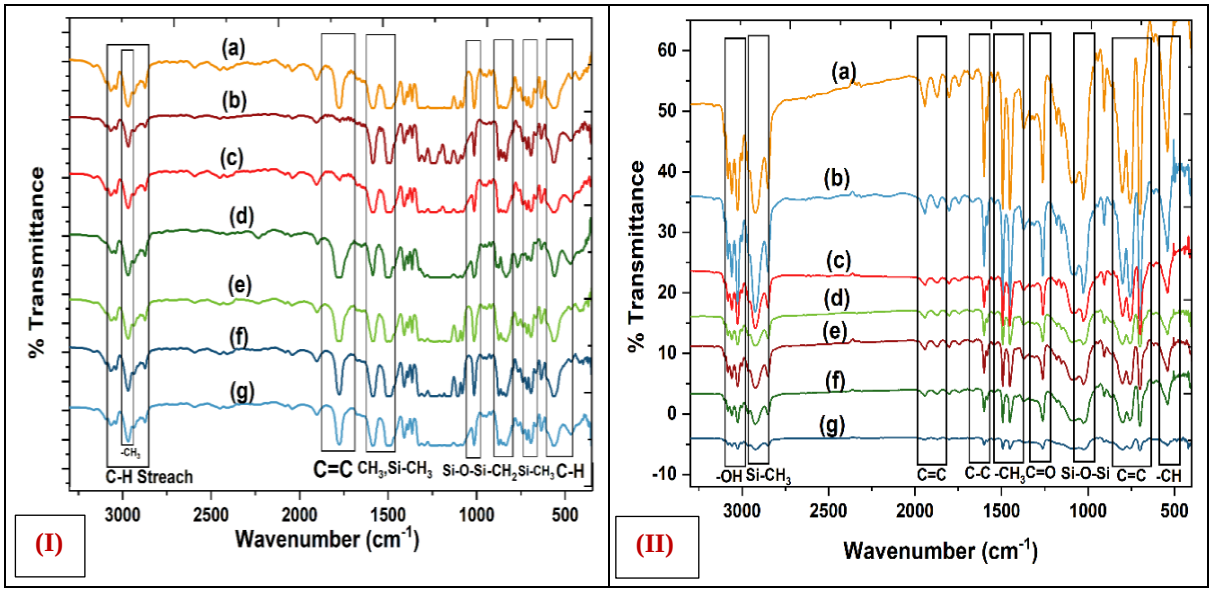

Figure 5.1.4: (I) FT-IR analysis of (a) $PS_{95}/PDMS_5$, (b) $PS_{90}/PDMS_{10}$, (c) $PS_{87}/PDMS_{13}$, (d) $PS_{85}/PDMS_{15}$, (e) $PS_{82}/PDMS_{18}$, (f) $PS_{80}/PDMS_{20}$, (g) $PS_{75}/PDMS_{25}$ and **(II)** FT-IR Spectra of (a) $PS_{75}/PDMS_{25}$ + 15 wt% of DES/CNT, (b) $PS_{75}/PDMS_{25}$ + 10 wt% of DES/CNT, (c) $PS_{75}/PDMS_{25}$ + 5 wt% of DES/CNT, (d) $PS_{75}/PDMS_{25}$ + 1 wt% of DES/CNT (e) $PS_{75}/PDMS_{25}$ + 15 wt% of CNT (f) $PS_{75}/PDMS_{25}$ + 10 wt% of CNT, (g) $PS_{75}/PDMS_{25}$ + 5 wt% of CNT

They shows the inorganic group absorption, maybe as a result of their limited presence in the PS/PDMS blend matrix [8,26]. The spectrum's lack of other bands other than those attributable to PDMS and the fact that the majority of them are still unchanged show purity of the polymers. On the other hand, the PS/PDMS acquired spectra showed the existence of additional peaks, including Si-O-Si (1008 cm^{-1}), Si-CH_3 (1619 cm^{-1}), and CH_2 and CH_3 (1860 cm^{-1}, 2957 cm^{-1}, and 2982 cm^{-1}) [26]. The medium intensity band, which occurred at 1710 cm^{-1} of CH_3, Si-CH_3 and corresponds to the vibration of its flexion. The different wt% used to make the PS/PDMS blend affects the strength and clarity of these signals. Given that the carbonyl group's signal strength decreases in the PS/PDMS blend, especially at greater inorganic component contents, it has assumed that this polymer group is responsible for the interaction between the two phases [26]. In additional studies that verified the creation of a urethane linkage with a band stretch at 3130 cm^{-1} overlapped with -OH stretching, a similar outcome was obtained. The unique bands of urethane linkages, which has been seen at 3130 cm^{-1}, which seem to overlap the -OH stretching vibration, verified their increasing output [24]. Peaks of -CH_3 deformation vibration in PDMS are between 1480 cm^{-1} and 1520 cm^{-1} and for PDMS, the multi-component Si-O-Si stretching peaks are seen between 1140 cm^{-1} and 1240 cm^{-1}. As shown in Figure 5.1.4 (II), there are two primary pathways for the generation of volatile linear and cyclic siloxane products during the heat de-polymerization of any PDMS containing materials. The first process entails backbiting a silanol (Si-O-H) chain end, followed by cyclization and removal of the cyclic product, and a shorter silanol ended linear chain.

The peak at 930 cm^{-1} experiences a little decline and swings to lower wavenumbers as CNT concentration in PDMS increases. Additionally, as seen in Figure 5.1.4 (II), the ratio between the two transmission values at 730 cm^{-1} and 790 cm^{-1} decreases as the CNT and DES/CNT concentration increases. As this impact has also shown for other carbon material-based composites, this is in excellent accord with the literature. Si-O-Si bands and Si-CH_3 rocking peaks are seen in the 1140 cm^{-1} and 2970 cm^{-1} regions, respectively. Furthermore, the symmetrical stretching mode of the C-H band in the methyl groups has been attributed to the band between 490 cm^{-1} and 530 cm^{-1}. The stretching vibration of C = O of carboxyl groups is responsible for the existence of DES/CNT at 1260 cm^{-1} that was also detected from analysis of TGA between the temperature range of 450 °C to 550 °C. Additionally, the FT-IR reveals that the oxidised functional groups on the CNT and DES/CNT are still there, which is important for the advancement of acoustic sound absorption technologies using these materials in the future.

5.1.3.5 Porosity and Thickness Analysis

Generally, pore size and porosity of membrane material depend on free volume available in the membrane matrix. Usually, rubbery composition has higher permeability with a low selectivity as their polymer chain segments are soft and can generate a larger fractional free volume (FFV) for the penetrants to transport. Due to their loose packing of the polymer chains and their random movements, allows the gas species to diffuse through the membrane matrix and in turn optimize the gas permeability [27]. On the other hand, if the FFV has reduced, the permeability can be denied too. Thus, the free volume has a direct effect on the gas permeability in polymers with respect to its solubility [28]. The introduction of PDMS into the glassy polymer matrix alters the porosity of the final membrane matrix structure [12,28]. PDMS, being a rubbery polymer, possesses higher mobility of its polymer chains as compared to the PS polymer chains [29]. This in turn gains the fractional free volume and improves the porosity of the resultant membrane. Figure 5.1.5 shows the percentage of porosity and thickness with respect to the blend composition. As per the data, the thickness remains almost constant, as the PDMS has used to add in the further blending.

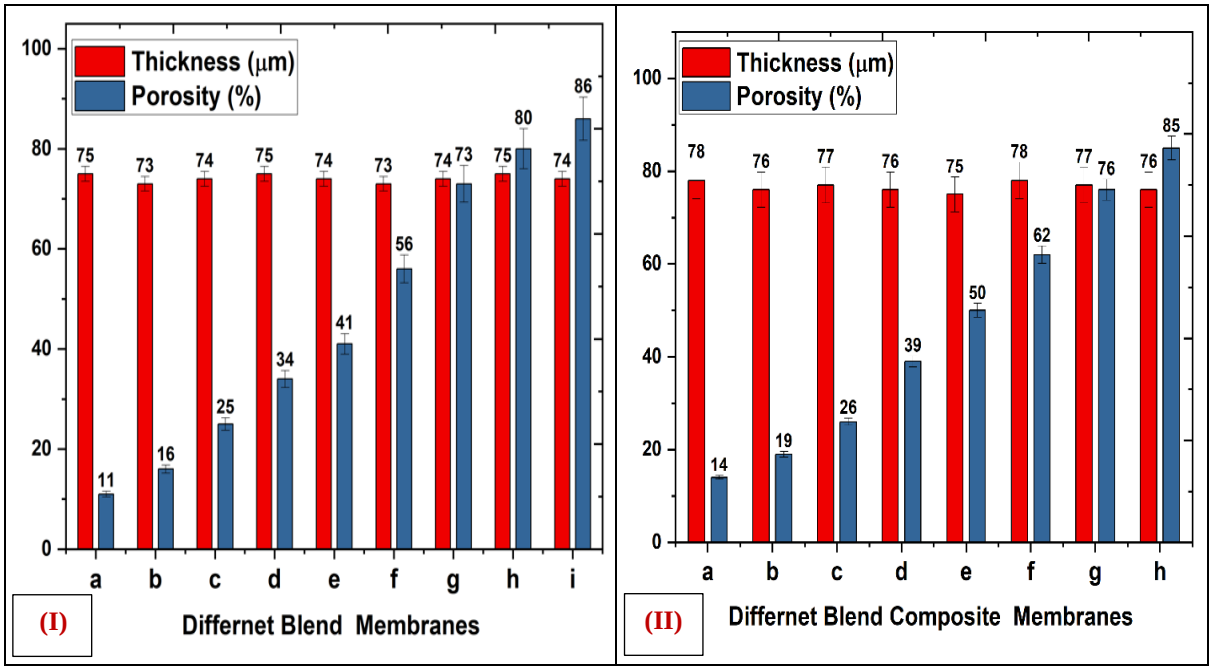

Figure 5.1.5: (I) Porosity and Thickness of different blend membranes of PS/PDMS polymer blends, (a) Pure PS, (b) $PS_{95}/PDMS_5$, (c) $PS_{90}/PDMS_{10}$, (d) $PS_{87}/PDMS_{13}$, (e) $PS_{85}/PDMS_{15}$, (f) $PS_{82}/PDMS_{18}$, (g) $PS_{80}/PDMS_{20}$, (h) $PS_{78}/PDMS_{22}$, (i) $PS_{75}/PDMS25$ and **(II)** Thickness and Porosity of blend membranes of PS/PDMS composites with different wt% of CNT and DES/CNT : (a) $PS_{75}/PDMS_{25}$ + 1 wt% of CNT, (b) $PS_{75}/PDMS_{25}$ + 5 wt% of CNT, (c) $PS_{75}/PDMS_{25}$ + 10 wt% of CNT, (d) $PS_{75}/PDMS_{25}$ + 15 wt% of CNT, (e) $PS_{75}/PDMS_{25}$ + 1 wt% of DES/CNT, (f) $PS_{75}/PDMS_{25}$ + 5 wt% of DES/CNT, (g) $PS_{75}/PDMS_{25}$ + 10 wt% of DES/CNT, (h) $PS_{75}/PDMS_{25}$ + 15 wt% of DES/CNT

The blending has not only enhanced the pore size of the final structure but also contributed to gain the porosity [32]. The porosity of the membrane is an important factor in determining how well it functions in all membrane separation methods. There are other methods to determine porosity, including mercury intrusion and gas adsorption, but the dry-wet weight technique is most suited for calculating the effective porosity of microporous membranes. The thickness and porosity of the membranes for the PS/PDMS-CNT and PS/PDMS-DES/CNT blend composites with different wt% of CNT and DES/CNT (1 wt%, 5 wt%, 10 wt%, 15 wt%) membranes are shown in Figure 5.1.5 (II). As shown in Figure 5.1.5 (II) the porosity increases with the amount of CNT and DES/CNT increases into PS/PDMS blend. The porosity of PS_{75}/$PDMS_{25}$-DES/CNT (15 wt%) is very high, as increasing the wt% of DES/CNT fillers in a blend of PS_{75}/$PDMS_{25}$ therefore the porosity increases significantly. In Figure 5.1.5 (II), the thickness of the membranes does not significantly change with increasing wt% of CNT and DES/CNT nanofillers. These results are consistent with previous studies that discovered that adding additional nanofillers to a material increased porosity and void size. Permeability increases with porosity increasing, and porosity is a measure of a empty spaces materials, while permeability is a measure of a capacity materials to transport gas molecules or fluids. Porosity and permeability inherent traits that all materials possess [30].

5.1.3.6 Solubility and Diffusivity

According to the solution diffusion model, as the gas molecules interact from the feed side, they are absorbed by the membrane surface and then diffuse throughout the thickness and lastly desorption takes place from the downstream side across the membrane. Therefore, solubility and diffusivity are the unintegral parameters of the gas transport process. Figure 5.1.6 (I) shows the diffusivity of various gases with blend membranes and it has shows from the results that this parameter has improved as the PDMS amount is increased. Even for the lower sorbing gases like O_2, N_2 and CH_4, the solubility has enhanced in a vast amount. As per the results, the increased amount of PDMS makes the gas species more diffused with the polymer chains which can be indicated by the data. In addition, from the DSC analysis, PS_{75}/$PDMS_{25}$ has higher T_g just due to increase of siloxane linkage which makes the composition more polar [31]. The enhanced polarity catalyzes the sorption of gas species. The highest gain can be noticed in CH_4 gas as it changes from 0.05 to 23.18 for pure PS to PS/PDMS blend with 25 wt% of PDMS. This gain is around 463 times due to blending [32]. Moreover, compared with N_2 diffusivity for pure PS which is more than the CH_4 diffusivity

for the same material. However, as the PDMS is increased up to 25 wt%, CH_4 diffusivity jumps above the N_2 diffusivity for the same material. The change has been observed for H_2 gas where the sorption parameter changes from 0.2 to 87.33, which is around 436 times. For O_2, the gain is about 172 times and for Ar it is 167 times. N_2 has also given a drastic change in the diffusivity even though it gives a hydrostatic compressive effect with the rubbery environment. N_2 solubility has also altered 120 times compared to the pure PS value. CO_2 diffusivity could not be determined from this experiment, as the diffusivity calculation has done from the solubility data obtained from the time lag method. However, in this case, there is no time lag for CO_2 gas [33]. This might be due to the higher condensability of CO_2 with the rubbery phase, gas permeation has carried forward without a time lag. On the other hand, H_2, being smaller in kinetic diameter, permeates faster without time lag. Another noticeable remark is that the gain in the diffusivity attributes to the gain in the wt% of PDMS. Thus, as the rubbery component is increases, the diffusivity also has been gained for each penetrant. It cannot be denied that the sorption is an unintegral parameter of permeability and it also depends on the penetrant shape as referenced by M. S. suleman et. al., [12]. Literature suggest, linear and flatten penetrants diffuse faster as compared to the spherical penetrants of equal mean diameter [34]. Generally, in glassy state, penetrant shape does not show significant effect whereas in the rubbery environment, it has long been known. The orientation of linear gas molecules through a polymer matrix in a direction along their axis reduces the displacement required of the polymer chains [35]. In this work, most of the penetrants are linear except CH_4 which has tetragonal structure, sorption of the other gases is larger compared to CH_4 solubility. Even though rubbery vicinity reduces the solubility of applied mass, it does not show a drastic reduction compared to their diffusivity. Solubility of the penetrant usually depends on the fractional free volume in the polymer matrix and it is higher in the glassy state. This can be confirmed by the results shown in Figure 5.1.6 (II) in which the solubility coefficient reduces with gain in wt% of PDMS. The diffusivity increases in the same manner for blends. However, the diffusivity varies in a less amount compared to solubility. This might accord with the phenomenon of weak size sieving of PDMS for which diffusion often changes less as compared to solubility variation. In addition, in a glassy/rubbery blend, the glassy domain in a rubber neatwork induces local strain as well as comprehensive force on the domain which forms reduction in the micro-void component to sorption [36]. Comparing the results for all the gases applied for the test diffusivity, CH_4 gives the lowest solubility.

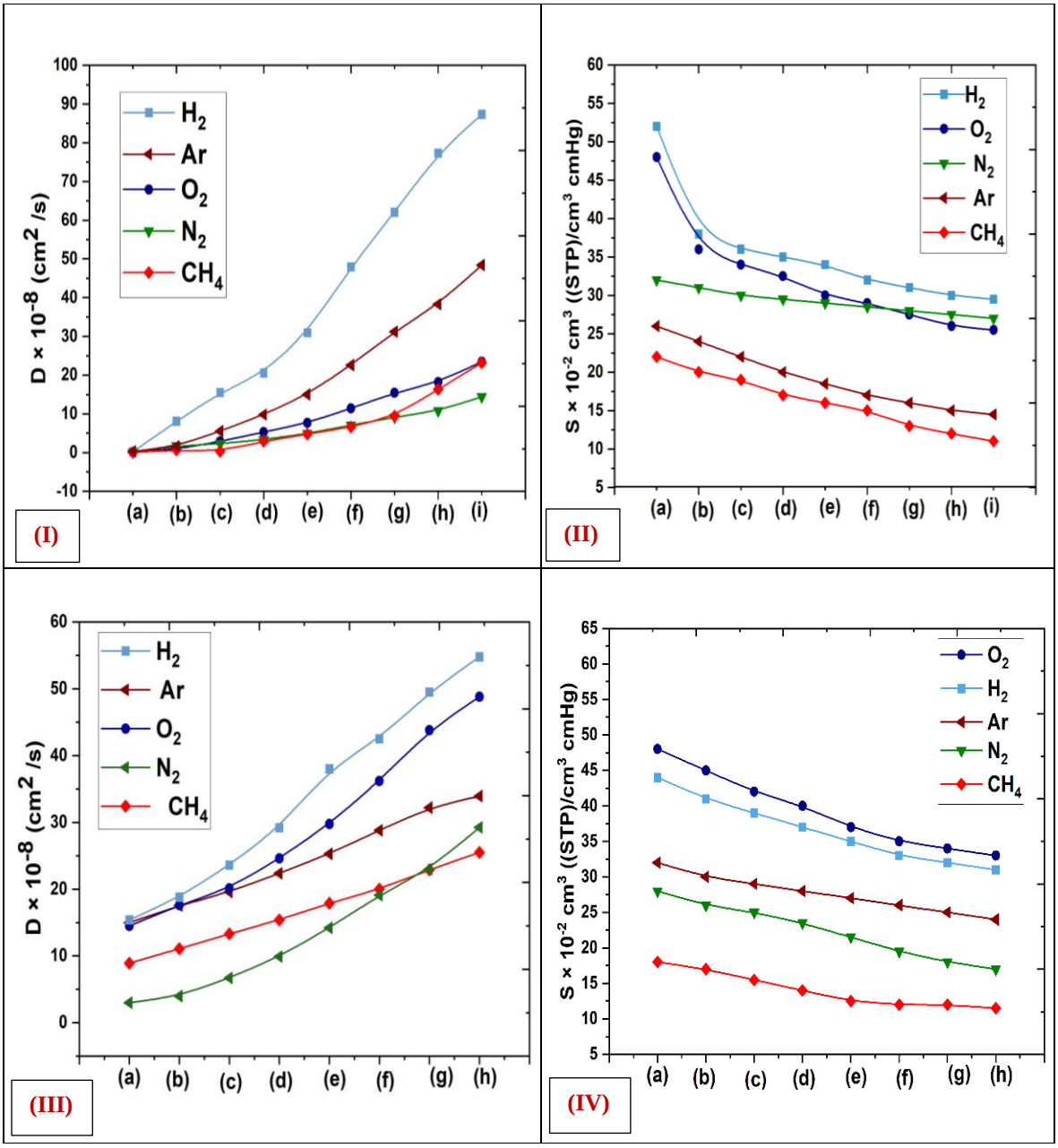

Figure 5.1.6: (I) Diffusivity and **(II)** Solubility of various blend membranes, here (a) Pure PS, (b) $PS_{95}/PDMS_5$, (c) $PS_{90}/PDMS_{10}$, (d) $PS_{87}/PDMS_{13}$, (e) $PS_{85}/PDMS_{15}$, (f) $PS_{82}/PDMS_{18}$, (g) $PS_{80}/PDMS_{20}$, (h) $PS_{78}/PDMS_{22}$, (i) $PS_{75}/PDMS_{25}$ and **(III)** Diffusivity and **(IV)** Solubility of Blend Composite Membranes of (a) $PS_{75}/PDMS_{25}$ + 1 wt% of CNT, (b) $PS_{75}/PDMS_{25}$ + 5 wt% of CNT, (c) $PS_{75}/PDMS_{25}$ + 10 wt% of CNT, (d) $PS_{75}/PDMS_{25}$ + 15 wt% of CNT, (e) $PS_{75}/PDMS_{25}$ + 1 wt% of DES/CNT, (f) $PS_{75}/PDMS_{25}$ + 5 wt% of DES/CNT, (g) $PS_{75}/PDMS_{25}$ + 10 wt% of DES/CNT, (h) $PS_{75}/PDMS_{25}$ + 15 wt% of DES/CNT

Even it reduced twice for the highest PDMS volume into PS compared to pure PS. H_2 solubility reduces around 1.76 times as the PDMS is added about 25 wt%. Moreover, the other gases also give reduction in the solubility as the amount of PDMS has increased [36]. Further, the solubility is reduced almost linearly according to the gain in the PDMS wt% in the PS

blend. As the rubbery phase has introduced into hard glassy phase, the chain mobility becomes more flexible which in turn, restricts the sorption of gas molecules [37]. However, a small decrement in the solubility coefficient has been recorded for the gas species. For N_2 gas, this parameter remains almost constant as the hydrostatic compressibility parameter plays the role. For Ar gas, it also reduces in the same manner as the other gases. Comparing both solubility and diffusivity plots, solubility gains as per the kinetic parameter of the gases whereas the reduction in the sorption of the same penetrants does not follow the trade. A noticeable remark for the CO_2 in this experiment is that it showed a steady permeation. Therefore, its time lag could not obtain and as a consequence its diffusion as well as the solubility was not determined.

The diffusion coefficient follows the trend in accordance with kinetic diameter of gases as the H_2 having smallest kinetic diameter diffuses faster as compared to CH_4. Usually, it is essential to get the CNTs well dispersed into polymer matrix structure. Usually, it is essential to get the CNTs well dispersed into polymer matrix structure. As the CNT and DES/CNT amount increases, it forms an agglomeration effect which in turn catalyses a 'channel flow'. Therefore, a highly discriminative passage arises within the smooth CNT surface or within the inner CNT tube [38]. Moreover, the nano-channels of CNTs also generate interfacial gaps with the polymer phase which is called external nano-channels. These nano-channels are interconnected throughout the entire membrane composition termed as direct channels (direct channels). These two factors play a key role to improve penetrant diffusion within the composite membrane. Generally, diffusion coefficients in the MMMs mainly relay on free volume created by the static cavities forms due to inefficient packaging of the polymer chains [37,38]. Moreover, the transient spaces are generated by the rearrangement of the thermally induced chain segments. The loading of CNT and DES/CNT develops such micro apertures to promote diffusivity of the gas molecules. As a consequence, all the gases have gained their diffusion coefficient with suitable composition. Figure 5.1.6 (I), suggests diffusivity of the penetrants uplifts by loading of CNT and DES/CNT in the PS/PDMS blend. However, CO_2 diffusivity could not be calculated as it did not show time lag during diffusion throughout the membrane thickness. These two factors play a key role to improve penetrant diffusion within the composite membrane [39]. As shown in Figure 5.1.6 (I), diffusion coefficient improves for all the penetrants used. At the beginning, by introducing wt% of DES/CNT the gases like H_2, Ar and O_2 shows almost the same diffusion coefficient. Meanwhile, by increasing the filler amount up to 15 wt%, diffusivity gains more than double for Ar gas and more than threefold value for H_2 and O_2 gases. CH_4 also shows variation around

three times by CNT loading. A drastic improvement can be seen for N_2 gas as its diffusivity uplifts more than 9 times for 15 wt% DES/CNT than 1 wt% loading of CNT.

The presence of CNTs into the blend polymer matrix changes the polymer-polymer interaction which in turn affects solubility, the physio-chemical factor that plays an important role in permeability and separation factor of MMM [39]. Solubility for PS/PDMS blend membrane increased as per our previous study but in this study, the introduction of DES/CNT has shown a reversed effect. Solubility coefficient for all the gases has reduced as shown in Figure 5.1.6 (II). The reduction in the solubility is almost in the same manner by increasing the loading for all the penetrants.

5.1.3.7 Permeability Analysis

Usually, rubbery composition has higher permeability with a low selectivity as their polymer chain segments are soft and can generate a larger fractional free volume (FFV) for the penetrants to transport. Due to their loose packing of the polymer chains and their random movements, allows the gas species to diffuse through the membrane matrix and in turn optimize the gas permeability [40]. Thus, the free volume has a direct effect on the gas permeability in polymers with respect to its solubility.

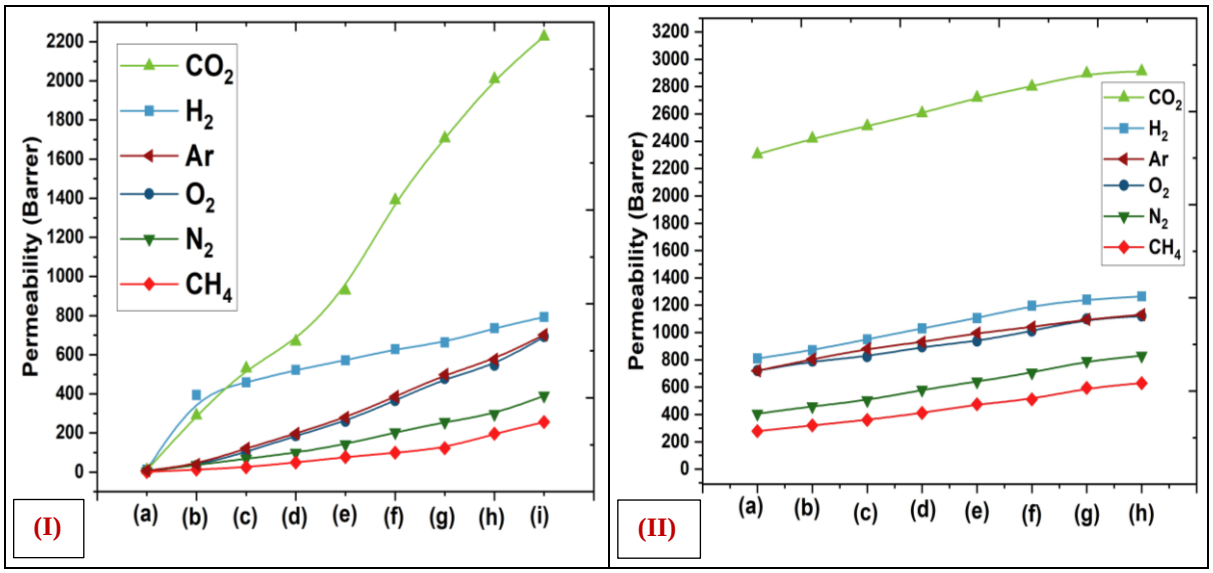

Figure 5.1.7: (I) Permeability of PS/PDMS blends (a) Pure PS, (b) $PS_{95}/PDMS_5$, (c) $PS_{90}/PDMS_{10}$, (d) $PS_{87}/PDMS_{13}$, (e) $PS_{85}/PDMS_{15}$, (f) $PS_{82}/PDMS_{18}$, (g) $PS_{80}/PDMS_{20}$, (h) $PS_{78}/PDMS_{22}$, (i) $PS_{75}/PDMS_{25}$ and **(II)** Permeability data of Blend Composite Membranes of (a) $PS_{75}/PDMS_{25}$ + 1 wt% of CNT, (b) $PS_{75}/PDMS_{25}$ + 5 wt% of CNT, (c) $PS_{75}/PDMS_{25}$ + 10 wt% of CNT, (d) $PS_{75}/PDMS_{25}$ + 15 wt% of CNT, (e) $PS_{75}/PDMS_{25}$ + 1 wt% of DES/CNT, (f) $PS_{75}/PDMS_{25}$ + 5 wt% of DES/CNT, (g) $PS_{75}/PDMS_{25}$ + 10 wt% of DES/CNT, (h) $PS_{75}/PDMS_{25}$ + 15 wt% of DES/CNT

Figure 5.1.7, shows the permeability has altered in a positive manner for all the gases applied for the gas permeation test as the PDMS weight percentages has been increased into the PS matrix. Moreover, in rubbery polymers like PDMS, there is a small change in diffusion coefficient compared to solubility coefficient for a group of penetrants, so that penetrants relative permeability largely depends on penetrants relative solubility [41]. Figure 5.1.7 indicates the variation in the gas permeability with respect to the penetrant as well different blending ratios and composite with CNT nanofillers. From the results, the introduction of PDMS into the glassy polymer phase gains the penetrant permeability. All the gases the change in the permeation follows the kinetic diameter of the gases except the CO_2 gas. There is a drastic change for CO_2 gas permeability, although it has higher kinetic diameter than H_2 and Ar gas molecules. Due to swelling of CO_2 with PDMS, polymer chain mobility increases which in turn gains the permeation of CO_2 gas molecules through the blend membranes having higher PDMS amount [40,41]. There is almost a linear gain in the permeability for all the gas species with respect to the introduction of PDMS into the PS matrix. Thus, the highest gain can be noticed for CO_2 gas as it has a condensable gas with the rubbery polymer phase. Therefore, by increasing the PDMS amount the CO_2 permeation also increases. A surprising outcome is that it gains beyond the gain for faster permeable gas like H_2. For pure PS, CO_2 permeability is 9.9 Barrer and as the blending is carried forward by adding PDMS, it reaches the highest value up to 2227 Barrer which is around 225 times gain compared to plane PS result. Moreover, as the PDMS is added with 5 wt% of total PS, CO_2 permeability increases from 9.9 Barrer to 290 Barrer. H_2, permeability changes from 12.77 Barrer to 793 Barrer, which is around 62 times increment [41]. For addition of 5 wt% of PDMS into PS, H_2 permeability jumps from 12.77 Barrer to 394 Barrer which depicts a drastic improvement due to introduction of a small rubbery amount into the glassy matrix. Furthermore, the other gases show more change for 25 wt% pf PDMS blend membranes compared to the pure PS with respect to H_2 gas. As the Ar gas results in the 90 times enhancement for the highest rubbery phase, i.e. increases from 7.76 Barrer to 702 Barrer. N_2 and O_2 permeability gains around 96 and 97 times respectively from pure PS to highest wt% gain. Another astonishing outcome has been detected for CH_4 permeability, which has improved from 1.25 Barrer to 255 Barrer for the virgin PS to 25 wt% of PDMS in PS which is around 207 times. Thus, in the case of CH_4, the modification in the membrane structure has altered its permeation compared to the faster permeable gases.

The ability of the membrane material to regulate the permeability of various species is essential for membrane separation. The penetrant initially dissolves in the membrane, diffuses

along the chemical potential gradient, and desorbs to the downstream side under the influence of the partial pressure difference. The solution-diffusion transport mechanism, a widely recognized explanation of gas permeation, describes how separation has been made possible by variations in the quantity of the penetrant that dissolves in the polymer and the rate at which the penetrant diffuses through the polymer. The solution-diffusion process affects gas permeation in polymer blend composite membranes. It can be inferred from the permeability plot that the introduction of CNT and DES/CNT into the blend membrane has improved permeability of all the applied penetrants. As the CNT amount has been increased into blend mixture, hydrophobic property improves which is confirmed by the contacts angle analysis. In addition, as referenced by X. Liu et. al. [32], CNTs dispersed into PDMS uplifts hydrophobicity of the composite membrane which in turn builds on the penetrant permeation with further addition of the fillers [32]. Usually, permeability of the MMM also improves due to increased active sorption sites within the blend membrane as the involvement of CNTs within the host polymer material generates catalytic centres [17]. In this case, DES/CNTs into the blend matrix create a near super hydrophobic surface which plays a key role to improve the penetrant permeability [18]. CNTs provide a large surface area to PS that turn result in a relatively weak interaction which uplifts the PS chain mobility [19]. The fabricated membranes contain a rubbery phase which has soft chain segments able to generate a larger fraction free volume (FFV) for the guest matter to transport. Even PDMS has loose packing as well as random movements, which promotes gas molecules to transport [20]. In addition, the introduction of CNTs into such a soft phase forms interfacial gapes as explained in the diffusivity parameter. Further addition of filler weight percentage continues with agglomeration and finally results in free volume which performs a key role to enhance gas permeability.

Figure 5.1.7 (II), shows gas permeability of all the gas species has improved as the DES/CNT and CNT weight percentages are increased into the blend composites. In the tested blend composite membranes, the enhanced gas permeability is attributed to the refined diffusivity rather than the solubility which is depicted in solubility and diffusivity plots [21]. The highest change can be observed in CO_2 permeation compared to other gases. CO_2 permeability upgrades in a dramatic manner as the amount of DES/CNT increases as compared to composites with only CNT nanofillers. Once again, there is a drastic improvement for CO_2 gas permeability, although it has higher kinetic diameter than H_2 and Ar gas molecules. This result attributes to swelling of CO_2 with PDMS phase; chain mobility alters which in turn gains the permeation of CO_2 within the membrane thickness [10]. Each gas species shows a linear

gain as the CNT and DES/CNT loading is improved. As the CNT and DES/CNT amount introduced from the lowest value 1 wt% to the highest 15 wt%, permeability of H_2, Ar and O_2 escalates to around 50%. A remarkable effect can be observed for N_2 and CH_4 as their gas permeability coefficient boosts more than the twofold value.

5.1.3.8 Selectivity and Trade-off Relationship

Gas separation of binary gas mixture through the membrane system depends on the gas species. Nevertheless, it also relies on the chemical interaction of gas molecules and the polymers. Usually, rubbery polymer membranes are solubility selective whereas the glassy polymer membranes are diffusivity selective [38]. Figure 5.1.8 (I) indicates the solubility selectivity of pure PS and PS/PDMS blends separation factor of various gases. It is clear from the Figure 5.1.8 (I) that the loading of PDMS has improved the solubility selectivity of all the gases. However, the trend does not follow the sequence as per the PDMS weight percentage. It shows the highest solubility selectivity for 20 wt% and 22 wt% of PDMS blends for almost all the gas pairs. Solubility selectivity has some significant difference for specific gas pairs as it changes according to the nature of polymer structure. Rubbery polymers have some higher solubility selectivity for O_2/N_2 whereas glass polymers have higher solubility selectivity for H_2/N_2 and H_2/CH_4 [27]. From the Figure 5.1.8 (I), solubility selectivity for H_2 with O_2, N_2 and CH_4 gives higher values as compared to the other gas pairs. It is obvious that the H_2 being a faster penetrant, its separation from the other gases gains with respect to the rest of gas pairs. Moreover, in almost all cases, except the N_2/CH_4 gas pair, solubility selectivity improves as the composition has transformed from pure glass to blend. PDMS with 90 wt% gives better solubility selectivity for all the gas pairs. On the other hand, in Figure 5.1.8 (II), diffusivity selectivity does not show any steady change as per the modification. For, H_2/O_2 gas pair, it almost remains constant, however the diffusivity selectivity reduces to a small extent with gain in the rubbery phase. For H_2/N_2 and O_2/N_2, only $PS_{75}/PDMS_{25}$, shows a significant gain and meanwhile as the membrane tends towards glassy phase, it shows a continuous reduction.

Separation of binary gas mixture within the membrane system depends on the kinetic diameter of gas species. For the H_2/CH_4 gas pair, pure PS and $PS_{75}/PDMS_{25}$ delivers a better result. However, it also relies on the physio-chemical interaction of gas molecules and the host polymers. Last but not the least, the N_2/CH_4 gas pair shows a continuous reduction in diffusivity selectivity with respect to the PDMS blending amount, which has observed in Figure 5.1.8 (II). In this study rubbery polymer PDMS is responsible for solubility selectivity whereas the glassy

polymer PS is responsible for diffusivity selectivity [38,39]. Furthermore, well-defined microporous cavities in the DES/CNT offer high gas-diffusion coefficients, whereas their ultra-microporous apertures contribute to high diffusion selectivity.

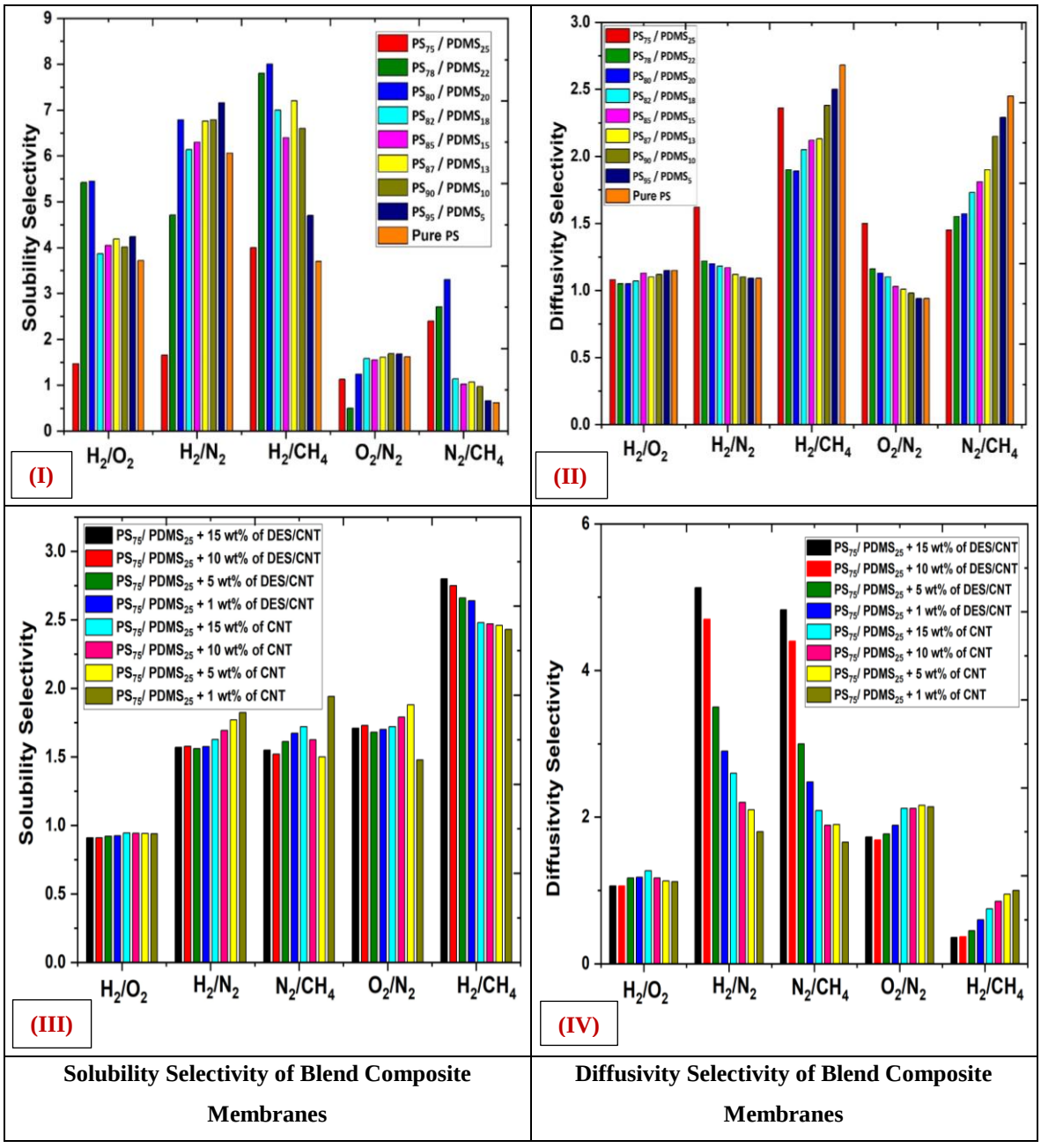

Solubility Selectivity of Blend Composite Membranes

Diffusivity Selectivity of Blend Composite Membranes

Figure 5.1.8: (I) Solubility selectivity and **(II)** Diffusivity selectivity of polymer blends of PS/PDMS with different wt% ratio **(III)** Solubility selectivity and **(IV)** Diffusivity selectivity of polymer blends composites of PS/PDMS-CNT with different wt% ratio of CNT

Figure 5.1.8 (III and IV) indicates the diffusivity selectivity and solubility selectivity of CNT and DES/CNT embedded PS/PDMS blend composite for various gas pairs. For the applied modification, selectivity of all the gasses improves as a consequence of introduction

of rubbery PDMS into glassy state. The mechanical properties also indicate the improved mechanical properties for separation of species. As the PDMS disperses within the voids and interface locations of PS, the resultant composition restricts a particular gas species which has finally improves the selectivity.

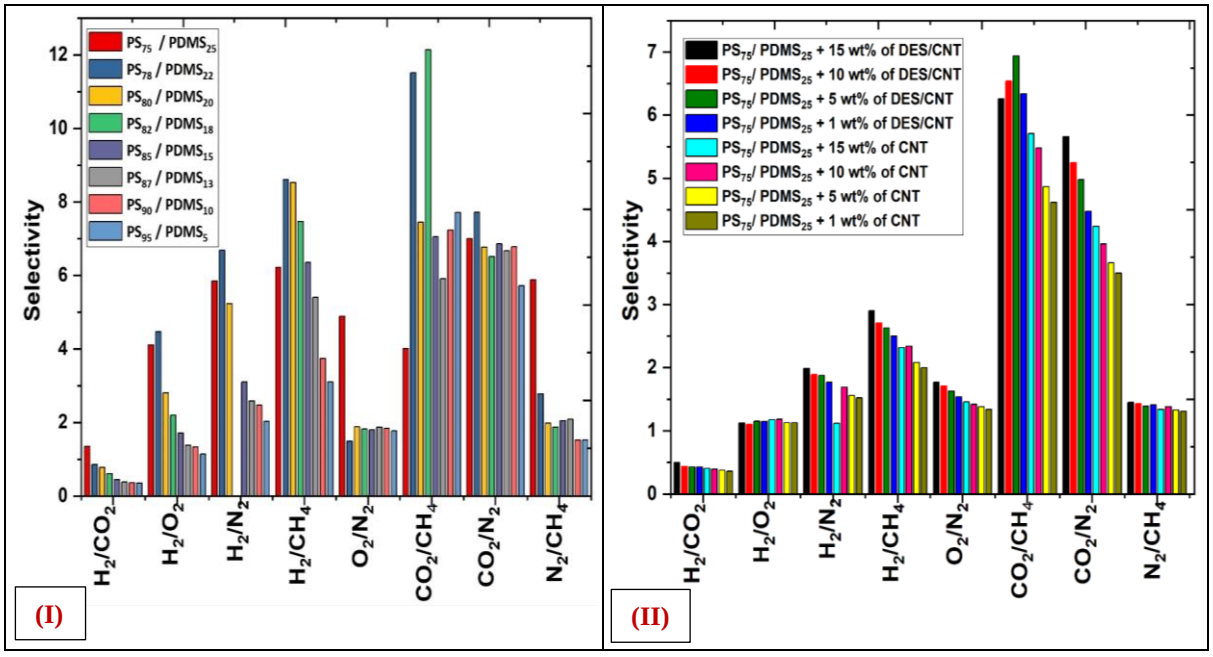

Figure 5.1.9: (I) Selectivity of polymer blends and **(II)** Selectivity of blend composite with CNT nanofillers

Separation of gasses has usually based on the nature of host membrane material. Glassy polymeric membranes dominate the position near or on the upper bound limit. Moreover, the rubbery composition lies to the left of the glassy composition and tries to tend towards the upper bound limit [5,7]. Figure 5.1.9 (I) shows the selectivity of gasses with respect to the blend ratio. There is a common noticeable thing for all the gasses along with every blend ratio, as the rubbery composition has enhanced into glassy composition, the selectivity lies towards the left-hand side to the glassy material performance in the Robeson's plots.

It can be inferred from the plots that with increase in the filler concentration, the trend does not follow any specific sequence. However, the final permeability selectivity depicted in Figure 5.1.9 (II) has a trend that tends towards Robeson's upper bound limits. Starting from the hydrogen separation as shown in Figure 5.1.10, H_2 having smaller kinetic diameter, permeates faster as compared to the other gas species. The separation of H_2 from CO_2 has improved due to the introduction of PDMS into the PS matrix.

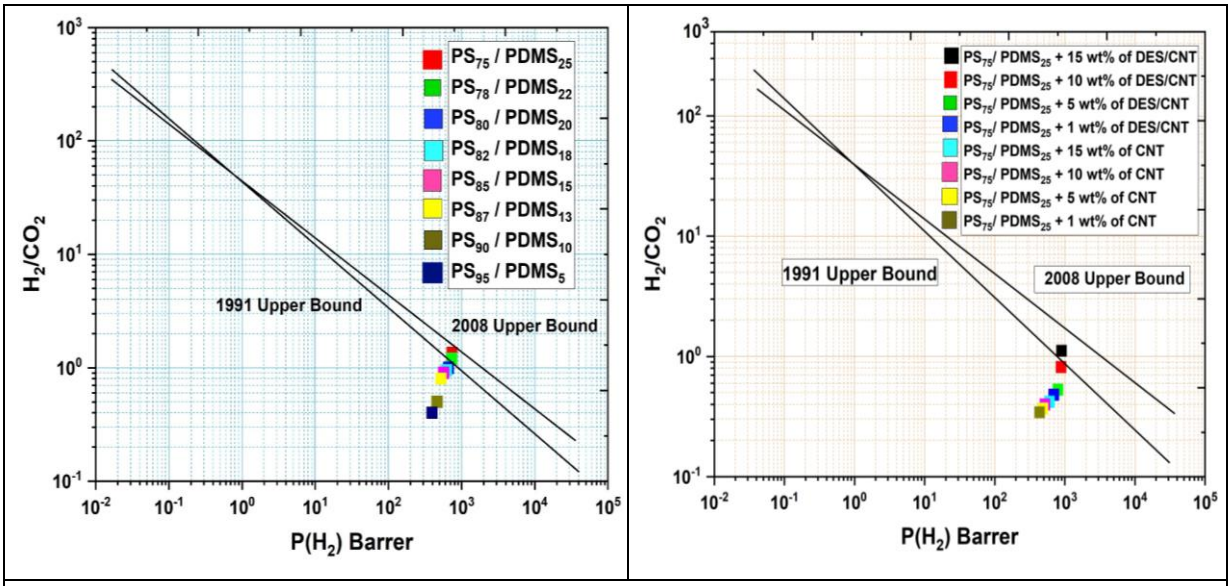

(I) Robeson's upper bound correlation for H_2/CO_2 separation

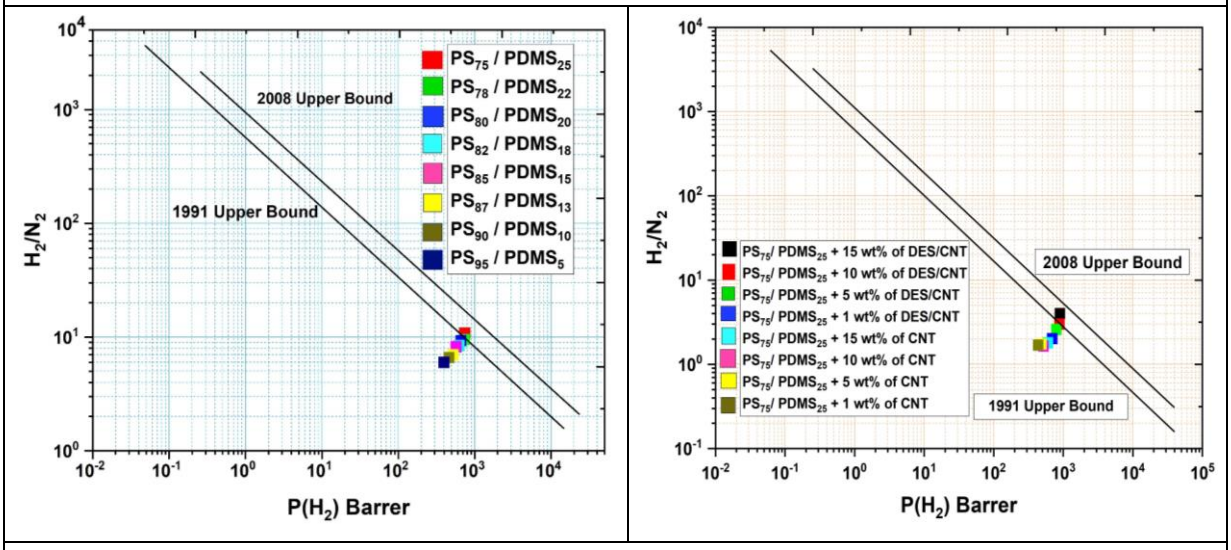

(II) Robeson's upper bound correlation for H_2/N_2 separation

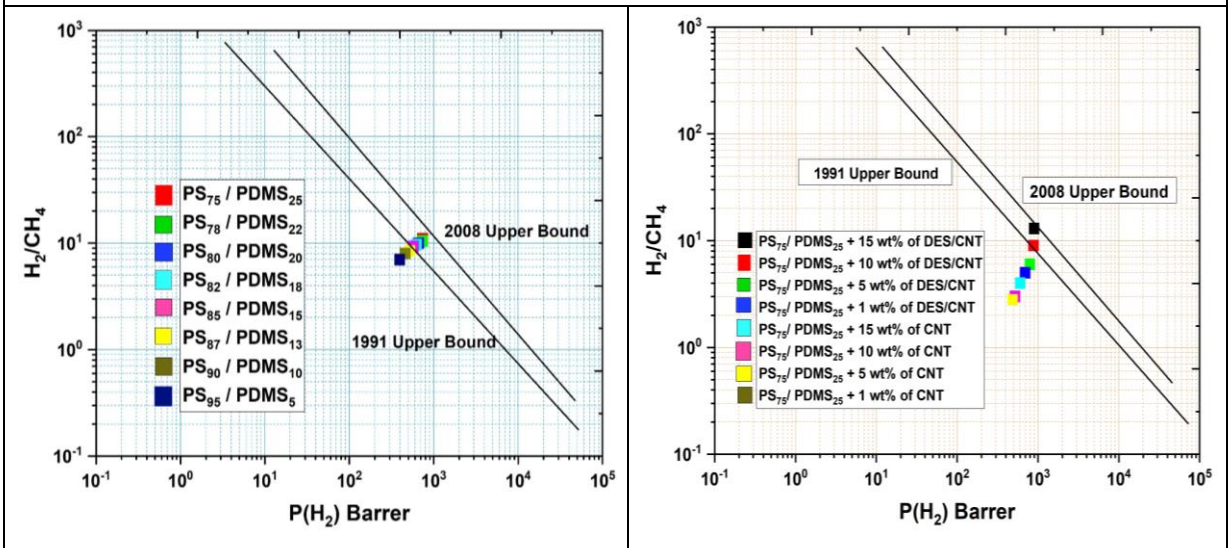

(III) Robeson's upper bound correlation for H_2/CH_4 separation

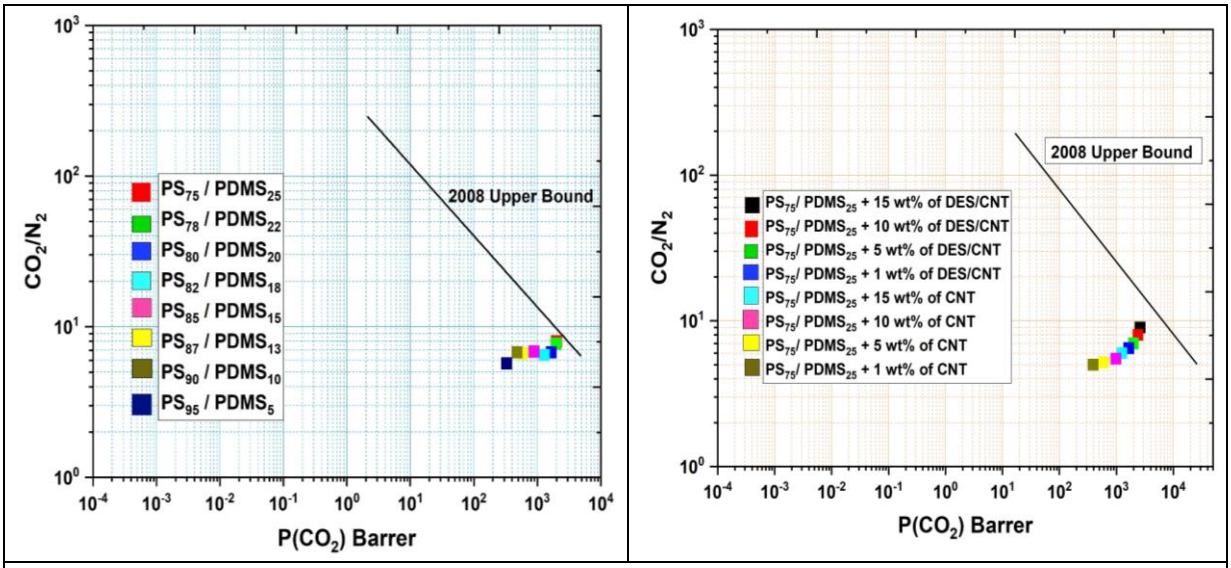

(IV) Robeson's upper bound correlation for CO_2/N_2 separation

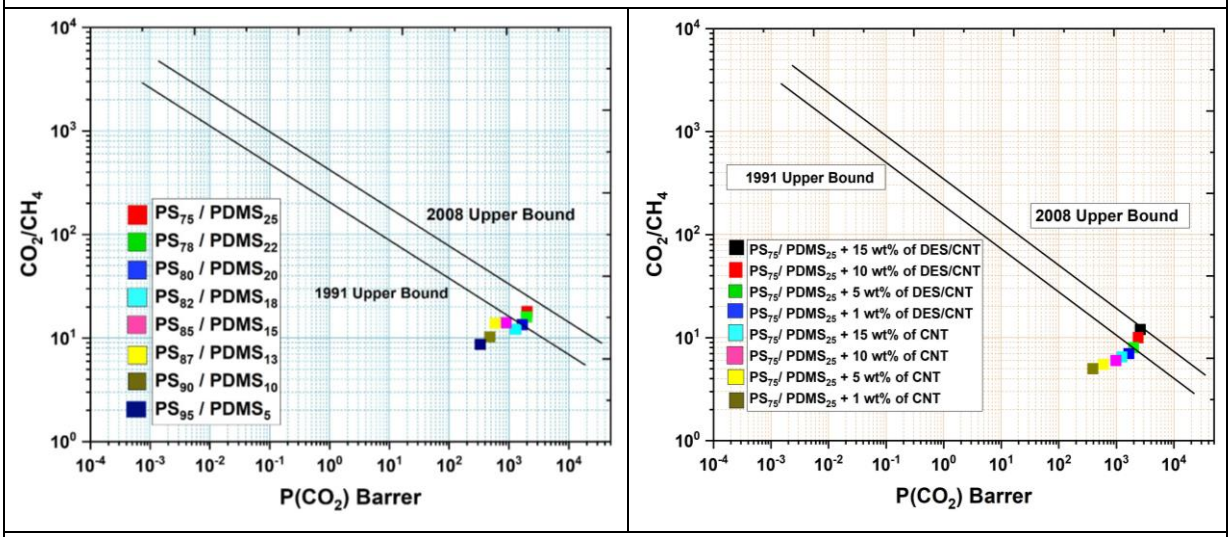

(v) Robeson's upper bound correlation for CO_2/CH_4 separation

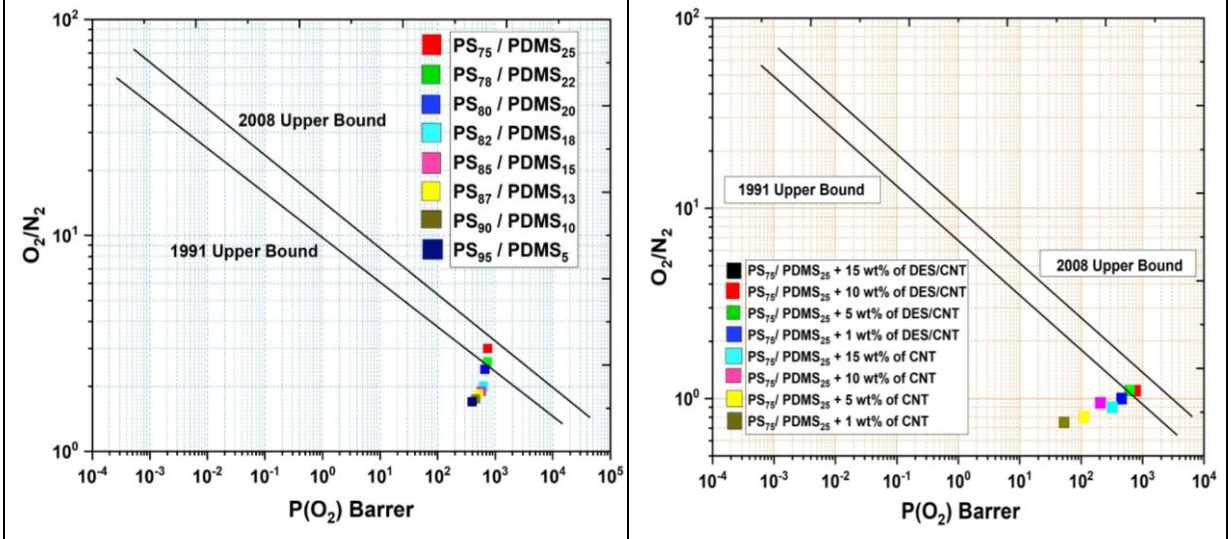

(VI) Robeson's upper bound correlation for O_2/N_2 separation

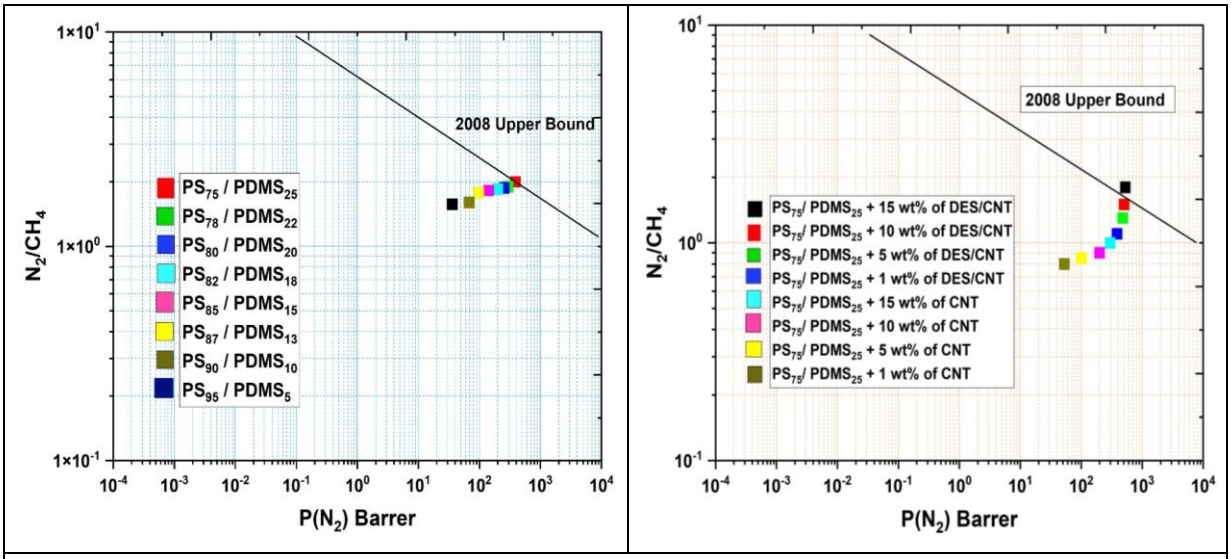

(VII) Robeson's upper bound correlation for N_2/CH_4 separation

Figure 5.1.10: Robeson's Plot of different PS/PDMS blends and PS/PDMS-CNT blend composites membranes with respect to different gas pairs ratios

As the amount of rubbery phase is increased, the selectivity is favored. The results can be compared with the Robeson's plot of H_2/CO_2 separation versus H_2 permeability as shown in the Figure 5.1.10 (I). It is clear from the plot that as the PDMS wt% has been introduced from 5 wt% to 25 wt%, the separation factor moves towards the Robeson's 1991 upper bound just lies on the same upper bound line for the highest PDMS [35]. As the kinetic diameter increases from H_2 to CH_4, selectivity also follows the same sequence, i.e. from H_2/CO_2< H_2/O_2< H_2/N_2< H_2/CH_4. Figure 5.1.10 (II) and Figure 5.1.10 (III) indicates Robeson's upper bound limits for H_2/O_2 and H_2/CH_4 respectively and in both these cases, the trend tends towards the boundary limit. Even in the case of H_2/CH_4 separation, the gain crosses the Robeson's 1991 limit and tends towards the 2008 plot boundary [34,39]. For 25 wt% of PDMS blends, the selectivity lies on the 2008 upper bound line, for 22 wt% of PDMS, the selectivity lies between 1991 and 2008 boundary limits and for 20 wt% of PDMS, it lies exactly on the 1991 plot [41]. These results may uplift hydrogen separation application for hydrogen recovery at large scale industrial applications. Moving towards CO_2 separation from N_2 and CH_4, blending has again improved the selectivity. Focusing on the CO_2/N_2 gas pair, the modified membrane has again given the results which makes them selective for CO_2 separation from N_2 gas. CO_2/N_2 selectivity for 22 wt% of PDMS has given the highest gain among all the blends for the same gas pair. Compared to plan PS, the blends have increased both permeability of CO_2 and N_2 as well the selectivity of CO_2/N_2. However, in the Robeson's plot shown in Figure 5.1.10 (IV),

the positions of the final compositions lies somewhat away from the plot limit. The enormous outcome can be noticed for CO_2/CH_4 separation for which the materials lie on the 1991 upper bound limit in Figure 5.1.10 (V). From the selectivity Figure 5.1.8, 22 wt% of PDMS gives the highest selectivity value. Separation of CO_2 from CH_4 does not show any steady change as the value fluctuates according to blend ratio. Even from the literature, it has confirmed that the inclusion of PDMS influences extra pores onto the membrane matrixes and catalases the CO_2/CH_4 separation [42]. For 25 wt%, 22 wt%, 15 wt% and 13 wt% of PDMS, the separation permeability value lies on the Robeson's 1991 upper bound limit. For the remaining gas pairs, the values are just tend towards the mentioned limit. Moreover, as referenced by D. F. Sanders, as per the nature of methane and CO_2, they behave differently with PDMS [36]. Usually, methane tries to compress the flexible polymer chain of PDMS under a particular feed pressure, whereas CO_2 swells the polymer matrix. N_2 separation from CH_4 has also proven the blends to be more selective compared to the pure glassy material. The selectivity for N_2/CH_4 increases more than twice by the introduction of 25 wt% of PDMS into PS matrix with respect to PS. In addition, the selectivity for N_2/O_2 gives good results in Robeson's plot for PS/PDMS blend materials, which has observed from Figure 5.1.10 (VI). Not only for this particular weight percentage but also for the remaining blends, it gives satisfactory results. In the Robeson's upper bound of 2008, 22 wt% and 13 wt% of PDMS blends lie exactly on the boundary limit. Even for the rest of the samples, it reaches to the limit in case of N_2/CH_4 as shown in the Figure 5.1.10 (VII) [35,39].

As the penetrant concentration of DES/CNT is increased up to 15 wt%, H_2/CO_2 selectivity just lies on the Robeson's 1991 plot given by Figure 5.1.10 (I). Diffusivity selectivity and solubility selectivity for H_2/O_2 gas pairs almost remain steady which results in the final output i.e. perm-selectivity also remain unchanged. Then after, for H_2/N_2 gas pair, selectivity due to diffusion gives a robust change. Nevertheless, the solubility selectivity reduces with a small variation. From the Figure 5.1.10 (II), 10 wt% and 15 wt% of DES/CNT nanofillers into blend matrix lead selectivity on Robeson's 1991 and 2008 plot limit. In the case of H_2/CH_4, a drastic change can be observed in solubility selectivity, which results in the highest value compared to other gas pair solubility selectivity. On the other hand, diffusivity selectivity reduces for this gas combination. Therefore, the outcome of H_2 separation from CH_4 is due to selectivity by the sorption parameter.

DES/CNT nanofillers amount plays a significant role in MMMs performance as the permeability and selectivity both improves with greater filler loading as compared to and CNT

nanofillers. This improvement is obtained as a consequence of disturbance of polymer chain packing which results in free volume content and flexibility of the membrane [40,41]. The nanoparticle loading at a certain value promotes agglomeration of fillers and results in a steep increment of gas permeability. The improvement in the gas perm-selectivity also results from the introduction of DES/CNT as disperses within the voids and interface locations of PS/PDMS, the resultant composition restricts a particular gas species which has finally improved the selectivity. Separation of gases are also based on the nature of host membrane material. Usually, glassy polymers dominate the position near or on the Robeson's upper bound limit.

5.1.3.9 FE-SEM Morphology and EDX

SEM provides ultra-high-resolution characterization and analysis giving precise, true nanometer scale information. It gives a resolution of 1.6 nm at 1 kv (TLD-SE) and <1 nm at 15 kV (TLD-SE). Figure 5.1.11 shows SEM micrographs of PS/PDMS-CNT blend composites with the 1 wt% lowest, maximum 15 wt% of CNT and 15 wt% of DES/CNT loading ratios. All of the developed membranes were dense and symmetric, as shown in Figure 5.1.11.

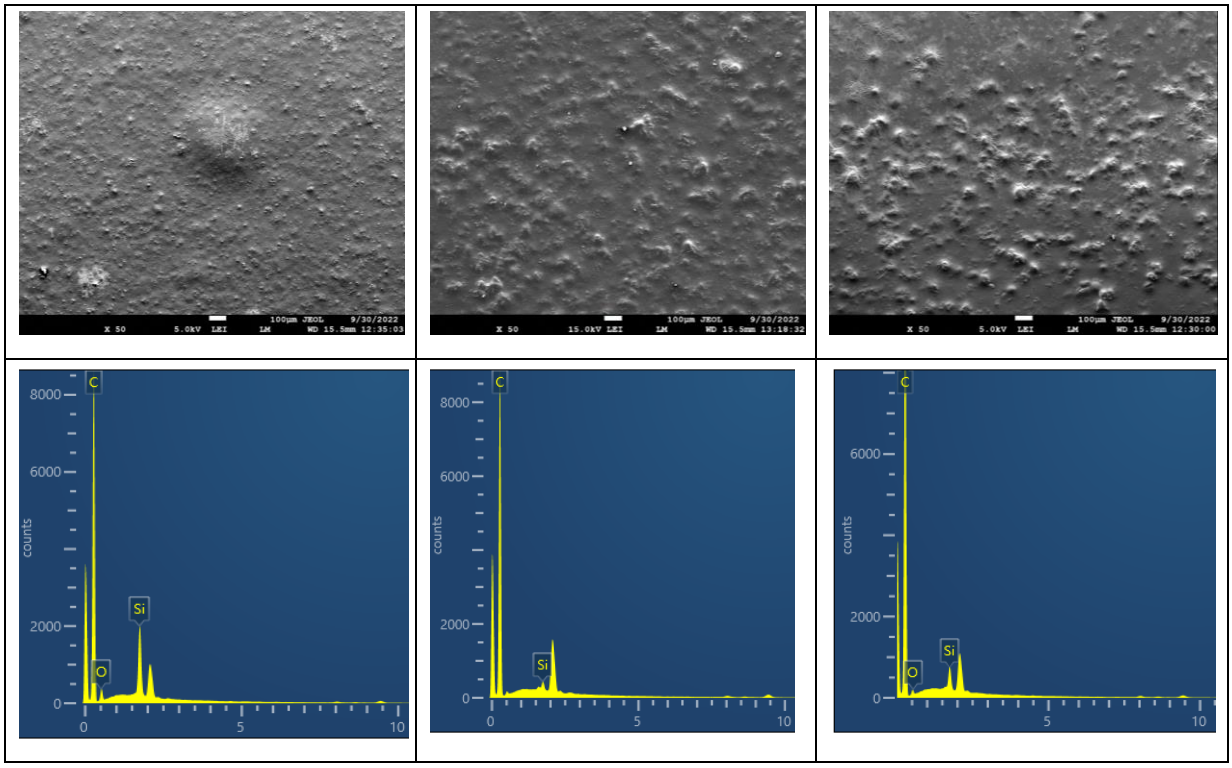

Figure 5.1.11: SEM images of **(I)** $PS_{75}/PDMS_{25}$ + 15 wt% of CNT, **(II)** $PS_{75}/PDMS_{25}$ + 15 wt% of DES/CNT, **(III)** $PS_{75}/PDMS_{25}$ + 1 wt% of CNT

The dispersion of composites membranes on a nanometric scale was further validated by SEM images [42]. In addition, CNT and DES/CNT nanofillers agglomeration at the polymer filler interface occurred, as shown by Figure 5.1.11, and several CNT dense area bundles has seen in the composite samples [43]. CNT particles generate significant aggregation portions in the PS/PDMS blend with a greater loading ratio of CNT nanofillers. The SEM picture shows several large-sized agglomerated nanoparticles in addition to nanofillers. The elemental makeup of the developed CNT and DES/CNT nanofillers was determined using the energy-dispersive X-ray (EDX). Figure 5.1.11 shows a surface with a smooth appearance to represent thick polymer blend composite membranes. Due to the blend with PDMS during the synthesis of the membrane, the EDX test shows a minor intensity peak of silica in the blend composite membranes of PS/PDMS- (CNT and DES/CNT). When blend of PS/PDMS composites with CNT and DES/CNT nanofillers, the dispersed microsphere of the carbon and silica particle was seen in PDMS as shown in Figure 5.1.11, and their existence was verified by the significant intensity peak of C and Si in blend composites membranes with increasing the wt% of CNT nanofillers in PS/PDMS polymer blend the amount of carbon is also increases and amount of Si has decreases which in observed form EDX spectra.

Table 5.1.2: Elemental analysis of PS/PDMS blends composites with different wt% of CNT and DES/CNT by using EDX

Elements	**$PS_{75}/PDMS_{25}$-CNT (1 wt%)**	**$PS_{75}/PDMS_{25}$-DES/CNT (15 wt%)**	**$PS_{75}/PDMS_{25}$-CNT (15 wt%)**
	Weight %	**Weight %**	**Weight %**
O	73.2	72.5	72.1
C	26.6	27.3	27.7
Si	0.2	0.2	0.2

There are some bigger particles due to the aggregation or overlapping of smaller particles. The SEM images show that the grains are spread randomly and are smaller. It is also noticeable that the particles have a uniform spherical shape. The analysis indicated that the sample exclusively included O and C particles, confirming its high purity and the lack of any other impurities [44]. Figure 5.1.11 presents the EDX spectra and elemental composition of these membranes along with corresponding SEM images of the selected membrane surface.

The oxygen content decreased from 73.2% in $PS_{75}/PDMS_{25}$-CNT (1 wt%) to 72.1% in $PS_{75}/PDMS_{25}$-CNT (15 wt%), which is observed from Table 5.1.2. Furthermore, carbon content increased from 26.6% to 27.7%, confirming the partial and progressive increment of CNT in the blend of PS/PDMS. Moreover, silica content remains 0.2% in $PS_{75}/PDMS_{25}$-CNT composite membrane, due to CNT nanofillers overlapping PS/PDMS polymer blend. The surfaces of 1 wt% of CNT membranes are smoother than those of 15 wt% membranes, as shown in Figure 5.1.11, and with increasing weight percentages of CNT, the $PS_{75}/PDMS_{25}$-(CNT and DES/CNT with 15 wt%) composite membranes become more roughened with wrinkles. $PS_{75}/PDMS_{25}$-(CNT and DES/CNT) composite membrane, which has a thin active layer of CNT with a thickness of around ~75 μm on top of the polymeric substrate layer and several micro voids within, is visible in the SEM image of these membranes.

5.1.4 Conclusion

This chapter concludes that the immense change has been observed in gas permeation and selectivity by found to be membrane modification in different ways. The mechanical capacity of all three PS/PDMS blend ratios are better than those of virgin polymer. In comparison to other PS/PDMS blends, the $PS_{75}/PDMS_{25}$ blend has higher tensile, flexural, and impact strengths. In addition, it has observed that the mechanical properties of the $PS_{20}/PDMS_{80}$ blends, including stiffness and toughness, were similarly found to be well balanced. The DSC test measures glass transition temperature to show the degree of miscibility. It has observed that PS and PDMS are miscible across the entire composition range. $PS_{75}/PDMS_{25}$ is optimized the preferred membrane due to its high hydrophobic caused by its high contact angle, high porosity, and high intensity of its siloxane group. The observation of membrane performances at raised solution temperature in this research advised that decreased macro voids at the bottom section of the membrane should be encouraged since industrial membrane operations needed high operating pressure and temperature.

It can be inferred from the results that a blend of rubbery and glassy polymers can combine high permeability as well as high selectivity, which can not be adopted by the single polymer membrane. The permeability steadily increases as the PDMS amount is raised from 1 wt% to 25 wt%. Moreover, enhanced permeability is due to the improved selectivity of the gas species with the blend membranes. A significant improvement in the permeability has been achieved for CO_2 gas, which is greater than H_2 gas permeability. Briefly, the study regarding blend-composites embedded with DES/CNTs improves overall gas transport parameters

compared to the virgin blend and composites with CNT nanofillers as were used in previous results. As per theoretical point of view, a small variation in DES/CNT amount introduces nanofillers, which in turn introduces free spaces into the blend matrix. These voids promote diffusion of gas molecules and finally overall enhances the penetrant transport within the hybrid membrane. Therefore, the improved permeability results due to gain in the diffusion coefficient. By increasing DES/CNT and CNT loading into blend composition separation performance of various gas pairs have inclined largely. By increasing the DES/CNT wt%, the final composition tends towards Robeson's upper bound limits of 1991 and 2008 which keeps them into the novel category of hybrid materials.

References:

[1] A. Hatami, I. Salahshoori, N. Rashidi, D. Nasirian, The effect of ZIF-90 particle in Pebax/Psf composite membrane on the transport properties of CO_2, CH_4 and N_2 gases by Molecular Dynamics Simulation method, *Chin. J. Chem. Eng.*, **2020**, 28, 2267–84.

[2] J. Park, H. Ha, H. W. Yoon, J. Noh, H. B. Park, D. R. Paul, et. al., Gas sorption and diffusion in poly(dimethylsiloxane) (PDMS)/graphene oxide (GO) nanocomposite membranes, *Polymer*, **2021**, 212.

[3] S. Wang, X. Li, H. Wu, Z. Tian, Q. Xin, G. He, et. al., Advances in high permeability polymer-based membrane materials for CO_2 separations, *Energy Environ Sci.*, **2016**, 9, 1863–90.

[4] X. Khanbabaei , E. Vasheghani-Farahani, A. Rahmatpour, Pure and mixed gas CH_4 and n-C 4H 10 permeation in PDMS-fumed silica nanocomposite membranes, *Chem. Engin. J.*, **2012**,191, 369–77.

[5] J. C. Jadav X, V. K. Aswal, H. Bhatt, J. C. Chaudhari, P. Singh, Influence of film thickness on the structure and properties of PDMS membrane, *J. Memb. Sci.*, **2012**, 415, 624–34.

[6] S. M. Jordan, W. J. Koros, Permeability of Pure and Mixed Gases in Silicone Rubber at Elevated Pressures, *J. of Poly. Phy.*, **1990,** 28, 795-809.

[7] L. M. Robeson, Q. Liu, B. D. Freeman, D. R. Paul, Comparison of transport properties of rubbery and glassy polymers and the relevance to the upper bound relationship, *J. Memb. Sci.*, **2015**, 476, 421–31.

[8] A. K. Patel, N. K. Acharya, Study of Gas Transport Phenomenon in Layered Polymer Nanocomposite Membranes, *Trends and App. in Advanced Poly. Materials*, **2017**, 25, 1123-40.

[9] H. D. Patel, N. K. Acharya, Transport properties of polymer blends and composite membranes for selective permeation of hydrogen, *Int. J. Hydro. Ener.*, **2023**, 15, 142-150.

[10] A. K. Patel, N. K. Acharya, Metal coated and nanofiller doped polycarbonate membrane for hydrogen transport, *Int. J. Hydro. Ener.*, **2018**, 21675–82.

[11] T. C. Merkel, V. I. Bondar, K. Nagai, B. D. Freeman, I. Pinnau, Gas Sorption, Diffusion, and Permeation in Poly(dimethylsiloxane) The permeability of poly(dimethylsiloxane) [PDMS], *J. of Poly. Phy.*, **2000**, 38, 108-20.

[12] M. S. Suleman, K. K. Lau, Y. F. Yeong, Enhanced gas separation performance of PSF membrane after modification to PSF/PDMS composite membrane in CO_2/CH_4 separation, *J. Appl. Polym. Sci.*, **2018,** 135.

[13] M. Kanduc, W. K. Kim, R. Roa, J. Dzubiella, How the Shape and Chemistry of Molecular Penetrants Control Responsive Hydrogel Permeability, *ACS Nano.*, **2021**, 15, 614–24.

[14] Z. Tian, S. Wang, S. Dai, D. Jiang, Effect of pore density on gas permeation through nanoporous graphene membranes, *Nanoscale*, **2018**, 10, 14660-14672.

[15] H. Ahmadizadegan, S. Esmaielzadeh, Fabrication and characterization of novel polyester thin-film nanocomposite membranes achieved by functionalized SiO_2 nanoparticles for gas separation, *Polym. Eng. Sci.*, **2019**, 59, 237–47.

[16] M. Pakizeh, M. R. Omidkhah, A. Zarringhalam, Synthesis and characterization of new silica membranes using template-sol-gel technology, *Int. J. Hydro. Ener.*, **2007**, 32, 1825–36.

[17] F. Orellana, J. Lisperguer, A. Perez-Guerrero, Synthesis and characterization of poly(methyl methacrylate)-silica, -Alumina and -Silica-Alumina Sol-Gel nanocomposites, *Macromolecules*, **2018**, 51, 21, 8522–8529.

[18] M. Goktas, J. Hacaloglu, Poly(methyl methacrylate) nanocomposites involving aromatic diboronic acid, *Polymer Bulletin*, **2019**, 76, 6231–43.

[19] M. Akmal, A. Raza, et. al., Effect of nano-hydroxyapatite reinforcement in mechanically alloyed NiTi composites for biomedical implant, *Materi. Sci. and Engin.: C*, **2016**, 68, 30-36.

[20] M. Abshirini, M. C. Saha, M. C. Altan, Y. Liu, L. Cummings, T. Robison, Investigation of porous polydimethylsiloxane structures with tunable properties induced by the phase separation technique, *J. Appl. Polym. Sci.*, **2021**, 138, 169-180.

[21] R. Guo, D. F. Sanders, Z. P. Smith, B. D. Freeman, D. R. Paul, J. E. McGrath, Synthesis and characterization of thermally rearranged (TR) polymers: Effect of glass transition temperature of aromatic poly(hydroxyimide) precursors on TR process and gas permeation properties, *J. Mater. Chem. A. Mater*, **2013**, 1, 6063–72.

[22] V. Mathur, K. Sharma, Thermal response of polystyrene/poly methyl methacrylate (PS/PMMA) polymeric blends, *Heat and Mass Transfer*, **2016**, 52, 01–11.

[23] A. K. Patel, N. K. Acharya, Thermally rearranged (TR) HAB-6FDA nanocomposite membranes for hydrogen separation, *Int. J. Hydro. Ener.*, **2020** , 45, 18685–92.

[24] D. Wang, D. Ba, Z. Hao Z, Li Y, Sun F, Liu K, et. al., A novel approach for PDMS thin films production towards application as substrate for flexible biosensors, *Mater. Lett*., **2018**, 221, 228–31.

[25] A. K. Zulhairun, Z. G. Fachrurrazi, M. Nur Izwanne, A. F. Ismail, Asymmetric hollow fiber membrane coated with polydimethylsiloxane-metal organic framework hybrid layer for gas separation, *Sep. Purif. Technol.*, **2015**, 146, 85–93.

[26] S. M. Lock, K. K. Lau, N. Jusoh, A. M. Shariff, C. H. Gan, C. L. Yiin, An atomistic simulation towards molecular design of silica polymorphs nanoparticles in polysulfone based mixed matrix membranes for CO_2/CH_4 gas separation, *Polym. Eng. Sci*., **2020**, 60, 3197–215.

[27] P. F. Cao, B. Li, T. Hong, K. Xing, D. N. Voylov, S. Cheng, et. al., Robust and Elastic Polymer Membranes with Tunable Properties for Gas Separation, *ACS Appl. Mater. Interfaces*, **2017**, 9, 26483–91.

[28] P. Bernardo, E. Drioli, G. Golemme, Membrane gas separation: A review/state of the art., *Ind. Eng. Chem. Res*., **2009**, 48, 4638–63.

[29] J. Zhang, J. Li, G. Jia, Y. Jiang, Q. Liu, X. Yang, et. al., Improving osteogenesis of PLGA/HA porous scaffolds based on dual delivery of BMP-2 and IGF-1: via a polydopamine coating, *RSC Adv.*, **2017**, 7, 56732–42.

[30] M. Iqhrammullah, M. Marlina, H. Khalil, K .H. Kurniawan, H. Suyanto, R. Hedwig, et. al., Characterization and performance evaluation of cellulose acetate-polyurethane film for lead II ion removal, *Polymers*, **2020**, 12, 226-242.

[31] J. F. Sark, N. Jullok, W. J. Lau, Improving the structural parameter of the membrane sublayer for enhanced forward osmosis, *Membranes*, **2021**, 11, 456-482.

[32] M. Abshirini, M. C. Saha, M. C. Altan, Y. Liu, L. Cummings, T. Robison, Investigation of porous polydimethylsiloxane structures with tunable properties induced by the phase separation technique, *J. Appl. Polym. Sci*., **2021**, 13, 1412-1436.

[33] X. Liu, J. Duan, J. Yang, T. Huang, N. Zhang, Y. Wang, et. al., Hydrophilicity, morphology and excellent adsorption ability of poly(vinylidene fluoride) membranes induced by graphene oxide and polyvinylpyrrolidone, *Colloids Surf. A. Physicochem. Eng. Asp.,* **2015**, 486, 172–84.

[34] G. Genduso, E. Litwiller, X. Ma, S. Zampini, I. Pinnau, Mixed-gas sorption in polymers via a new barometric test system: sorption and diffusion of CO_2-CH_4 mixtures in polydimethylsiloxane (PDMS), *J. Memb. Sci.*, **2019**, 577, 195–204.

[35] B. D. Freeman, Basis of permeability/selectivity tradeoff relations in polymeric gas separation membranes, *Macromolecules*, **1999**, 32, 375–80.

[36] L. M. Robeson, The upper bound revisited, *J. Memb. Sci*., **2008**, 320, 390–400.

[37] I. S. Tsagkalias, T. K., Manios, D. S. Achilias, Effect of graphene oxide on the reaction kinetics of methyl methacrylate in situ radical polymerization via the bulk or solution technique, *Polymers*, **2017**, 15, 165-182.

[38] D. F. Sanders, Z. P. Smith, R. Guo, L. M. Robeson, J. E. McGrath, D. R. Paul, et. al., Energy-efficient polymeric gas separation membranes for a sustainable future: A review, *Polymer*, **2013**, 54, 4729–61.

[39] C. A. Scholes, G. W. Stevens, S. E. Kentish, Membrane gas separation applications in natural gas processing, *Fuel*, **2012**, 96, 15–28.

[40] M. Bhattacharya, Polymer nanocomposites-A comparison between carbon nanotubes, graphene, and clay as nanofillers, *Materials*, **2016**, 14, 132-148.

[41] S. A. Mansoori, M. Pakizeh, A. Jomekian, CO_2 and H_2 selectivity properties of PDMS/PSf membrane prepared at different conditions, *Front Chem. Sci. Eng.*, **2011**, 5, 500–13.

[42] H. D. Patel, N. K. Acharya, Transport, Spectroscopic, and Electrical Properties of Thermally Rearranged Nanocomposite Membranes, *Chem. Eng. Technol.*, **2022**, 45, 2223–33.

[43] H. D. Patel, N. K. Acharya, Synthesis and characteristics of HAB-6FDA thermally rearranged polyimide nanocomposite membranes, *Polym. Eng. Sci*., **2021**, 61, 2782–91.

[44] A. K. Patel, N. K. Acharya. Study of gas transport phenomenon in layered polymer nanocomposite membranes, *Trends and App. in Adva. Poly. Materials*, **2017**, 191–206.

Chapter

5.2

DES/GO Doped PS/PDMS Nanocomposite Membranes to Enhance the Stability of CO_2/CH_4 Separation

Contents

Chapter – 5.2

DES/GO Doped PS/PDMS Nanocomposite Membranes to Enhance the Stability of CO_2/CH_4 Separation

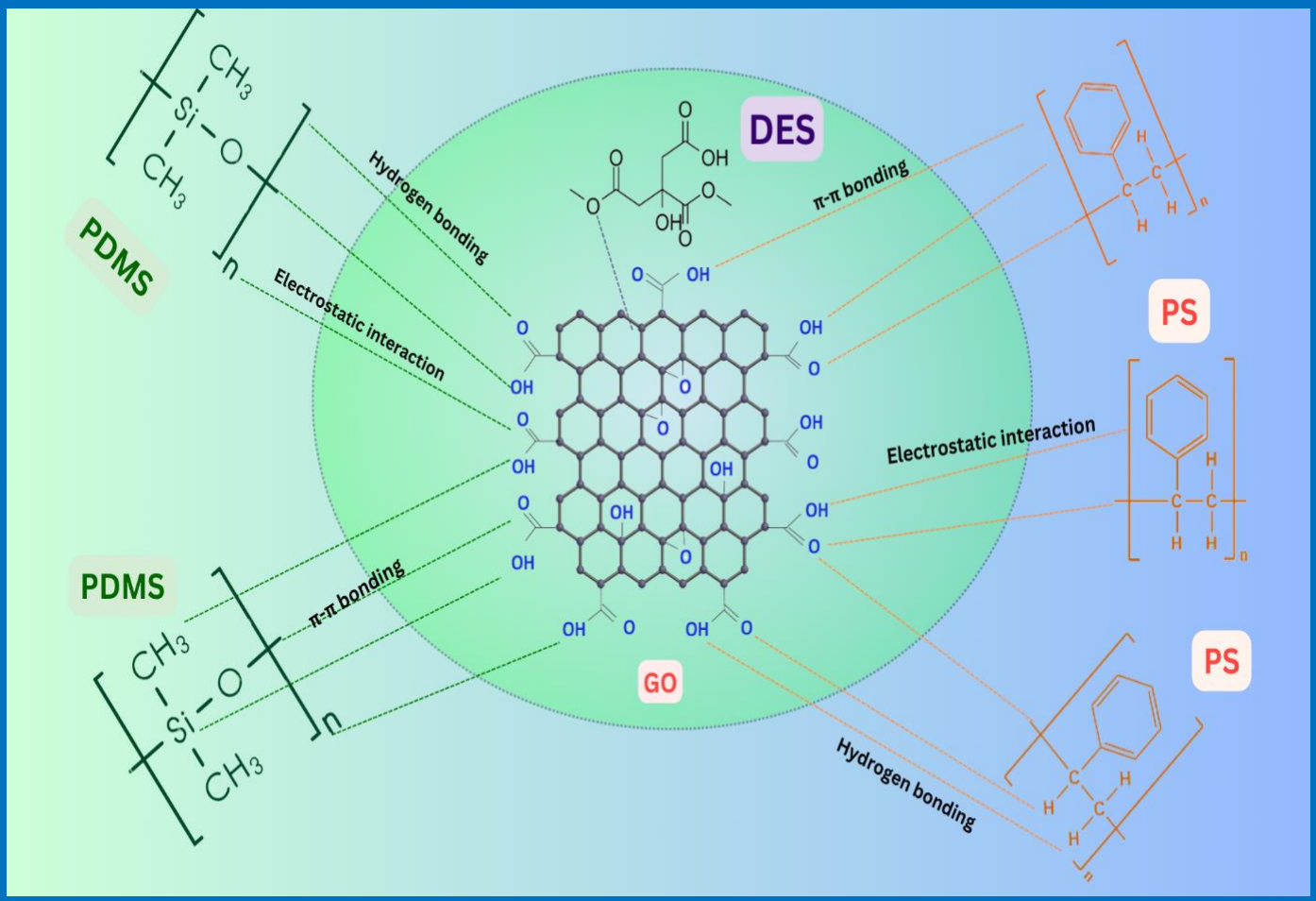

This chapter describes the improved performance of nanocomposite membranes. In this chapter blend-composites of polymer nanofillers and deep eutectic solvent (DES) based blend-composites membranes are characterized outlined using a single gas permeation method. Mixed Matrix Membrane (MMM) were prepared by using polydimethylsiloxane (PDMS), polystyrene (PS) blend and incorporate of graphene oxide (GO). The combination of glassy and rubbery polymers with GO nanofillers has been characterized by gas permeability for different wt% of GO and DES/GO nanofillers. The sorption and diffusion capacity of GO have been significantly improved the gas transport. In addition, DES coating to GO fillers boots the results were found beyond an empirical upper bound for H_2/CO_2 gas pair. Polymer nanocomposites (PNCs) membranes were synthesized using phase inversion technique and tested by using constant pressure/variable volume gas permeability system. Series of membranes were characterized by made using other standard techniques including Fourier Transform Infrared (FT-IR) Spectroscopy, Porosity analysis, Water Contact Angle, Differential Scanning Calorimetry (DSC) and Thermogravimetric Analyzer (TGA) to confirm the change in thermomechanical behavior.

5.2.1 Introduction

Deep Eutectic Solvents (DESs) are a class of ionic liquids that have gained significant attention in recent years as environmentally friendly and sustainable solvents. Unlike traditional solvents, which are often volatile organic compounds with potential environmental and health hazards, DESs are composed of a eutectic mixture of two or more components, typically a hydrogen bond donor (HBD) and a hydrogen bond acceptor (HBA). The low melting point is attributed to the strong hydrogen bonding interactions between the HBD and HBA components, leading to the formation of a eutectic system that remains in a liquid state at temperatures much lower than the melting points of the individual components [1]. DESs are often considered green solvents because they can be derived from natural, renewable resources. The combination of deep eutectic solvents (DES) and graphene oxide (GO) has found applications in diverse fields due to the unique properties of both components. It has verity of applications; the combination typically involves using a DES as an electrolyte or solvent and incorporating graphene oxide as a conductive additive or electrode material. Advantage of this combination capitalizes on the high conductivity of graphene oxide and the desirable solvent properties of the deep eutectic solvent, resulting in an electrolyte system with improved electrochemical performance [2].

The improved conductivity of graphene oxide contributes to the high power density of the super capacitor. Challenges include optimizing the synthesis methods for DES/GO, improving scalability, and addressing any limitations in terms of energy density and cycle life. The application of DES/GO in the gas separation technology as well electrochemical energy storage shows the synergistic benefits. This has the potential to contribute to the development of more efficient and environmentally friendly material for gas separation technology and energy storage devices [3].

5.2.2 Experimental

5.2.2.1 Membrane Synthesis and Characterization

PS and PDMS polymers were dissolved Dichloromethane for solution casting. GO nanofiller was individually stirred for 12 hr in a solvent of Dichloromethane, and then went the mixture of PS/PDMS blend composite with different weight percentage ratios of GO (1 wt%, 3 wt%, 5 wt% and 10 wt%) fillers was sonicated for 1 hr by using probe-sonicator to avoid agglomeration and then entire solution was again stirred for 24 hr at ambient atmospheric condition. DES was synthesized and characterized using the same procedure as reported previously. Mixed solution has been transferred in a round bottom flask and then stirrer at 80 ± (0.1) °C for 2 hr. The mixture was filtered and washed several times with distilled water by using ethanol (50 ml every time). This DES-modified nanocomposite (DES-GO) was dried in a vacuum oven for 24 hr at 80 ± (0.5)°C. Now these DES-GO nanofillers mixed with PS-PDMS blend and stirred for 2 hr. The solvent with PS/PDMS-GO (1, 3, 5 and 10 wt%) and PS/PDMS-DES/GO (1, 3, 5 and 10 wt%) was poured on a glass plate, and the solvent was left to evaporate overnight. Furthermore, the details of characterization techniques i.e. permeability, DSC, TGA, SEM, etc., have been discussed in chapter 2.

5.2.3. Results and Discussions

5.2.3.1 Solubility and Diffusivity

Pure gas permeability of various weight fractions of GO embedded and DES modified GO embedded PS/PDMS blend membranes were investigated at a constant feed pressure of 30 psi using constant pressure/variable volume system. To analyse the impact of incorporation of GO fillers in depth, physicochemical parameters were studied first. As a result of previous work, the introduction of PDMS into PS improved solubility of the penetrants and showed a small reduction in diffusion coefficient. However, here the results are quite different

as the filler amount increases, solubility losses and the diffusion coefficient improves in a drastic manner as shown in Figure 5.2.1 (I) and Figure 5.2.1 (II). It can be inferred from Figure 5.2.1 (I), that diffusivity for all the experimental gasses influences significantly as the GO stuffing. At first, the blend-composite membranes with various weight percentages (1 wt% to 10 wt%) of GO nanofillers gives improved diffusion coefficient. Nevertheless, 1 wt% of DES-GO embedded membrane alters higher diffusivity than the 10 wt% of GO into the blend matrix. Furthermore, as the DES coated GO proportion increases, the penetrant diffusion enhances [3].

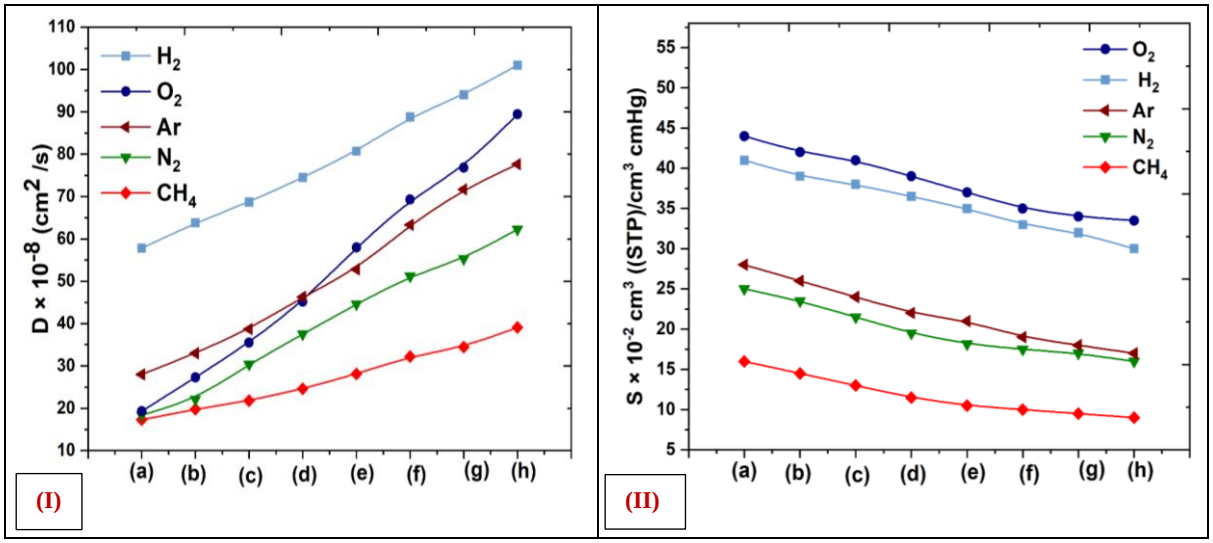

Figure 5.2.1: (I) Diffusivity and **(II)** Solubility of various blend composites membranes, (a) $PS_{75}/PDMS_{25}$ + 1 wt% of GO, (b) $PS_{75}/PDMS_{25}$ + 3 wt% of GO, (c) $PS_{75}/PDMS_{25}$ + 5 wt% of GO, (d) $PS_{75}/PDMS_{25}$ + 10 wt% of GO, (e) $PS_{75}/PDMS_{25}$ + 1 wt% of DES/GO, (f) $PS_{75}/PDMS_{25}$ + 3 wt% of DES/GO, (g) $PS_{75}/PDMS_{25}$ + 5 wt% of DES/GO, (h) $PS_{75}/PDMS_{25}$ + 10 wt% of DES/GO

Figure 5.2.1 (I), H_2 gas molecules diffuse faster compared to the other gasses. Fourfold increment was observed in coefficient by loading of GO from 1 wt% to 10 wt% of DES/GO. Here not only GO runs the show but DES affects significantly on diffusion parameter. According to the characteristics of GO flacks, it creates various tortuous channels for gas diffusion and these channels depend on the kinetic diameter of the gas molecule. In addition, due to the strong interface interaction within GO nanofillers and the host polymer, polymer chain mobility is restricted. As an outcome, the activation energy of the diffusing gas molecules increases. In addition, usually fillers mostly form interfacial voids between filler surface and the polymer phase resulting in fractional free volume. Therefore, as both the pristine GO and DES coated GO fraction is elevated, FFV escalates and boosts mass transport parameters. Usually, nanofillers tend to agglomerate with polymer phase being different in the characteristics, which in turn form free volume within the vicinity of the filler surface.

Moreover, diffusivity of MMMs rely on free volume created by the static cavities forms due to inefficient packaging of the polymer chains. According to Benworth B. Hansen, et. al., DES delivers intermolecular attraction to the diffusing gas molecules. Therefore, the adsorption capacity of the composite membrane improves [4]. On the other hand, solubility reduces with a smaller fraction for all the gasses compared to the gain in the diffusion coefficient. Nevertheless, there is a noticeable remark for O_2 gas solubility which follows the similar trend as other gases but it gives higher value than H_2 gas.

5.2.3.2 Permeability Analysis

The combination of rubbery and glassy polymer membrane influences gas permeability parameters due to the revised physical and chemical constituents. PS/PDMS blend membrane has proven to be selective for various gas pairs in previous work. However, the launch of pristine GO and DES modified GO into this blend composition regulate the transport behavior.

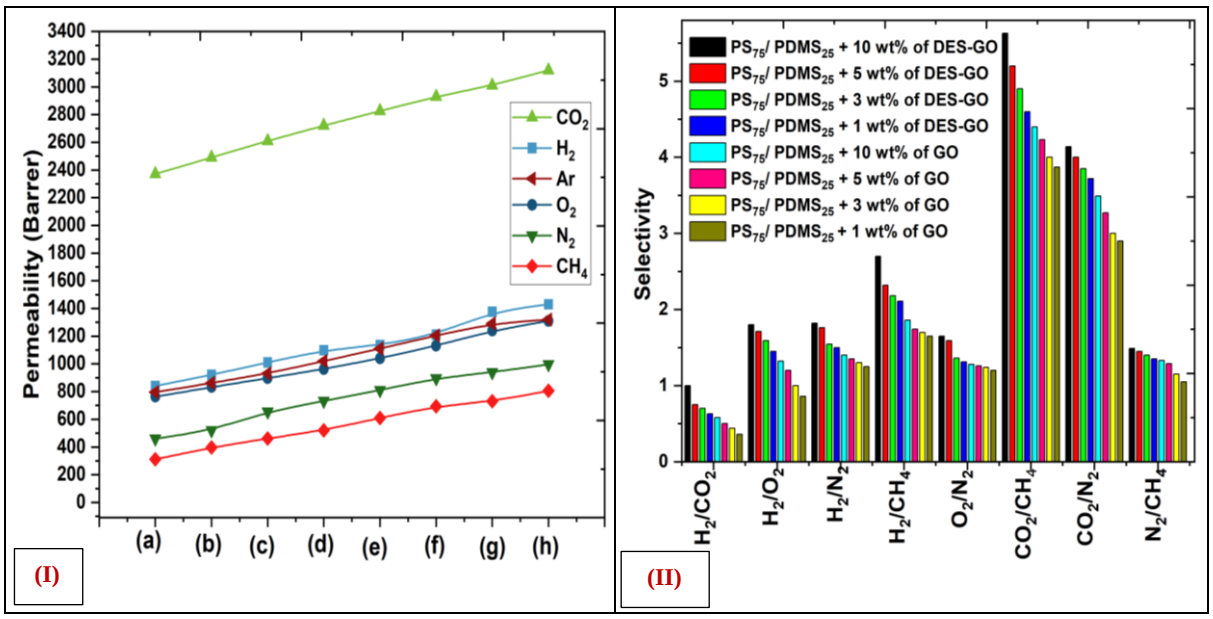

Figure 5.2.2: (I) Permeability and **(II)** Selectivity of various blend composites membranes, a) $PS_{75}/PDMS_{25}$ + 1 wt% of GO, (b) $PS_{75}/PDMS_{25}$ + 3 wt% of GO, (c) $PS_{75}/PDMS_{25}$ + 5 wt% of GO, (d) $PS_{75}/PDMS_{25}$ + 10 wt% of GO, (e) $PS_{75}/PDMS_{25}$ + 1 wt% of DES/GO, (f) $PS_{75}/PDMS_{25}$ + 3 wt% of DES/GO, (g) $PS_{75}/PDMS_{25}$ + 5 wt% of DES/GO, (h) $PS_{75}/PDMS_{25}$ + 10 wt% of DES/GO

Figure 5.2.2 shows the permeability of the feed gasses is enhanced as the filler loading of GO flacks increases from 1 wt% to 10 wt% and it further shows a linear gain as the DES coated GO amount is raised for the similar weight fractions. It can be scrutinized from the plot that only 1 wt% of DES-GO gains gas permeability of all the applied feed gasses than the 10 wt% of GO loading. However, CO_2 permeability results in an outstanding performance as it

enhances far better than the H_2 permeability. Generally, H_2 transports faster than CO_2 being smaller in the kinetic diameter but in this study CO_2 permeation is three-fold higher than H_2 permeation. Benworth B., reported the unique outcome is due to adsorption-desorption properties of CO_2 gas molecules [4].

Although CO_2 is a nonpolar gas, its individual C-O bonds interact with the carboxylic acid group of GO providing specific sorption sites to attract CO_2 molecules. Even the structural defects in the form of nano-pores located on the GO surface vigorously traps CO_2 molecules [3,4]. Hansen, et. al, reported that DES provides a platform for intermolecular attraction to the penetrating gas molecules and improves the adsorption capacity of the membrane material [4].

Table 5.2.1: Comparison of permeability of various polymer blend composites

Material	Permeability (Barrer)					
	H_2	**O_2**	**CO_2**	**N_2**	**CH_4**	**Ar**
Pure PS	12.77	7.08	9.9	4.04	1.23	7.76
$PS_{75}/PDMS_{25}$	793	692	2227	390	255	702
$PS_{75}/PDMS_{25}$ + 10 wt% of GO	1098	962	2720	732	520	1020
$PS_{75}/PDMS_{25}$ + 10 wt% of DES-GO	1430	1310	3121	996	805	1320

Comparative permeabilities results of the membrane modifications are as shown in Table 5.2.1. As compared to pure PS, PS/PDMS blend membranes give magnificent gas permeation for all the experimental gasses. Further modification by introducing 10 wt% of GO and DES-GO improves the permeability drastically.

5.2.3.3 Porosity and Thickness Analysis

The introduction of GO and DES/GO into the polymer blend alters the porosity of the final membrane matrix structure. The porosity of $PS_{75}/PDMS_{25}$ + DES/GO (1 wt% to 10 wt%) is quite significant. As we increased the wt% of DES/GO fillers in a blend of $PS_{75}/PDMS_{25}$, the porosity was dramatically enhanced, that type of results we are expecting this blending is very useful for such kind of hydrogen gas applications.

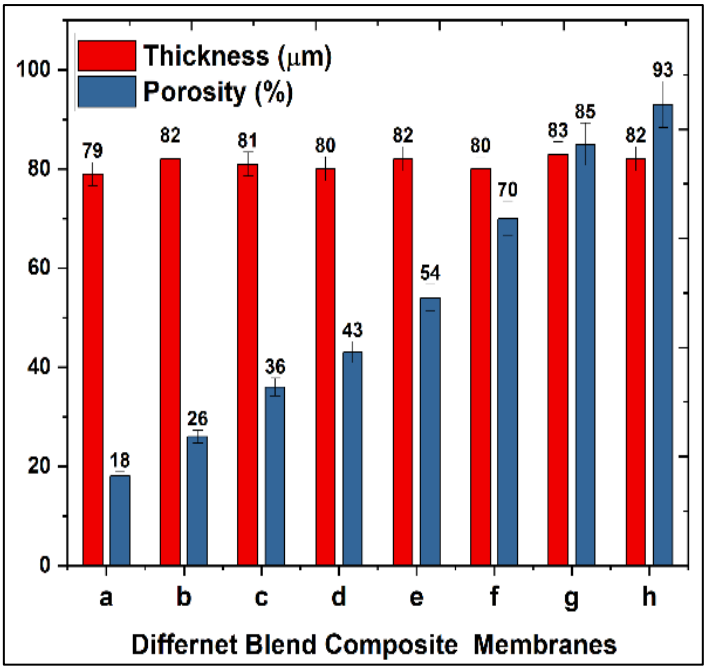

Figure 5.2.3: Thickness and Porosity, of (a) $PS_{75}/PDMS_{25}$ + 1 wt% of GO, (b) $PS_{75}/PDMS_{25}$ + 3 wt% of GO, (c) $PS_{75}/PDMS_{25}$ + 5 wt% of GO, (d) $PS_{75}/PDMS_{25}$ + 10 wt% of GO, (e) $PS_{75}/PDMS_{25}$ + 1 wt% of DES/GO, (f) $PS_{75}/PDMS_{25}$ + 3 wt% of DES/GO, (g) $PS_{75}/PDMS_{25}$ + 5 wt% of DES/GO, (h) $PS_{75}/PDMS_{25}$ + 10 wt% of DES/GO

The thickness of the membranes did not substantially change when changing the weight percentages of the GO and DES/GO nanofillers in either Figure 5.2.3, which means in our study the thickness of a membrane cannot play a key role in the measurement of permeability of membranes [8]. The results obtained that porosity of materials and void size increased when additional nanofillers were added.

Porosity is a measure of voids of materials, while permeability is a measure of a capacity of material to transport gas molecules or fluids. As porosity increases permeability also increases. The porous structure with smaller pores shown a greater ability to sustain flow stress when the number of holes along the width increased by increasing the weight percentage of DES/GO.

Alternatively, samples with larger pore sizes exhibited more deformation than samples with lower pore sizes, indicating a more flexible behavior of material.

5.2.3.4 Selectivity and Trade-off Analysis

Rubbery polymers have higher solubility selectivity whereas glassy phase supports diffusion selectivity [5]. In this work, blend matrix is composed of both glassy as well as rubbery polymer chains along with filler composition. Therefore, the selectivity will depend on the effect of filler composition. According to the physicochemical parameters of the resultant membrane, diffusion coefficient is responsible for the gas permeation as it increases with respect to filler weight fraction. Therefore, separation of binary gas mixture would depend on diffusivity selectivity. Figure 5.2.4 (I and II) indicate separation factor, diffusivity selectivity and solubility selectivity respectively. It is deduced from the plots that as the filler content is raised, selectivity is improved which is attributed to diffusivity selectivity. Although solubility selectivity reduces, its magnitude covers a smaller fraction compared to diffusivity selectivity have the result favors the separation factor for all the gas pairs.

Concerning the separation of H_2 from the mixture of gasses, selectivity of the gas pairs increases in order of $H_2/CO_2 < H_2/O_2 < H_2/N_2 < H_2/CH_4$. This is due to the difference in the kinetic diameter of H_2 with kinetic diameter of the other gases. In addition, the trade-off relationship is also plotted and shown in Figure 5.2.4 (III to VIII). Specifically, for H_2 separation, the DES-GO composite membranes have crossed Robeson's 1991 upper bond and tend towards 2008 upper bond. H_2 diffuses faster relative to other gasses through GO derived nano-channels. Nevertheless, the rest of the gasses cannot pass via the nano-channels. It may be due to increase by GO fillers, provides additional diffusion pathways to the H_2 and CO_2 gas molecules. The smaller kinetic diameter gas molecules can swiftly pass through the empty spaces whereas the larger kinetic diameter gas molecules accumulate within the interlayer gallery of GO. Similarly, for the rest of the gas pairs, membrane modification offers a fruitful selectivity. However, CO_2/CH_4 selectivity is the highest one among all the gas pairs. This might be due to a specific interaction of CO_2 and the hydrocarbon gas with the host membrane compositions. Therefore, such kind of membrane composition is applicable in natural gas purification, carbon dioxide capturing and fuel gas treatment where CO_2 is separated from methane and nitrogen [6]. Due to adsorption-diffusion characteristic of CO_2 with GO in MMM, it diffuses faster than the other gasses. Additionally, functional groups of DES catalyze separation as well as permeability of CO_2 in MMM because of its affinity for CO_2.

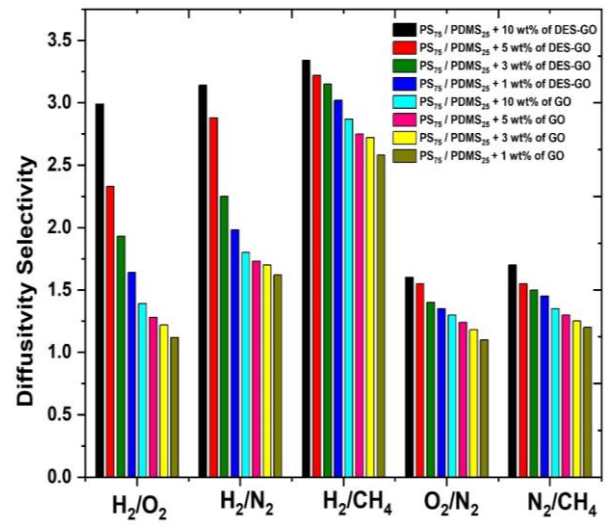

(I) Diffusivity Selectivity of Blend Composite

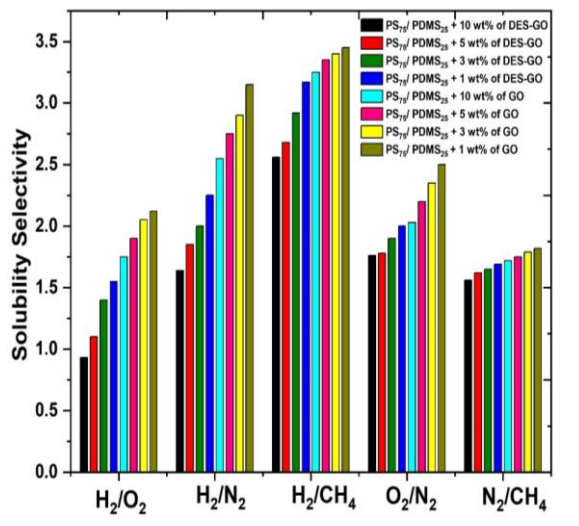

(II) Solubility Selectivity of Blend Composite

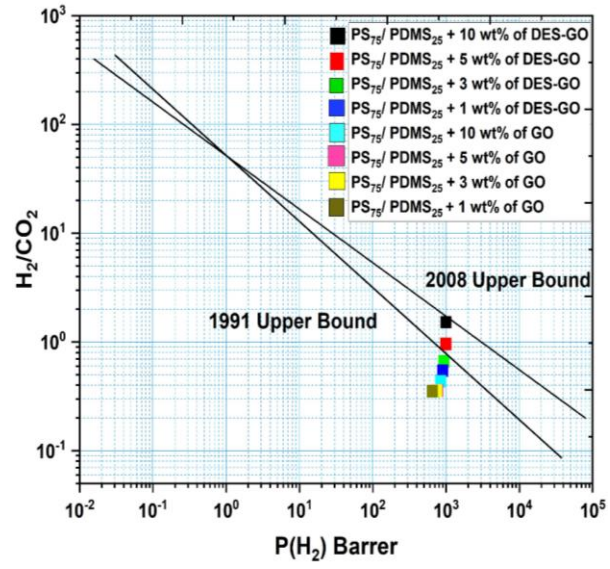

(III) Robeson upper bound for H_2/CO_2

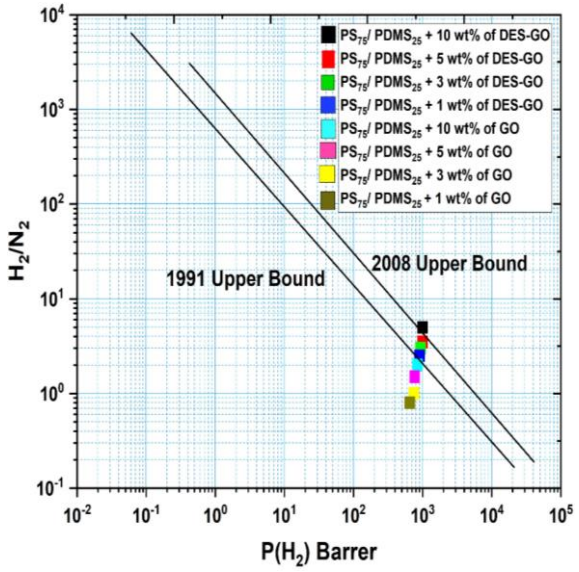

(IV) Robeson upper bound for H_2/N_2

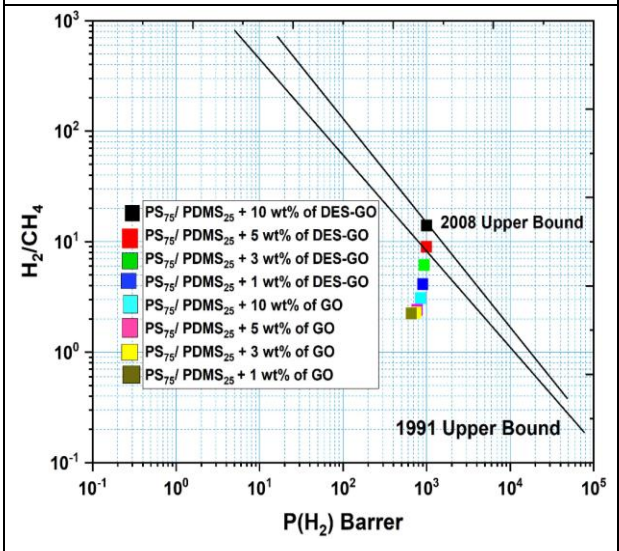

(V) Robeson upper bound for H_2/CH_4

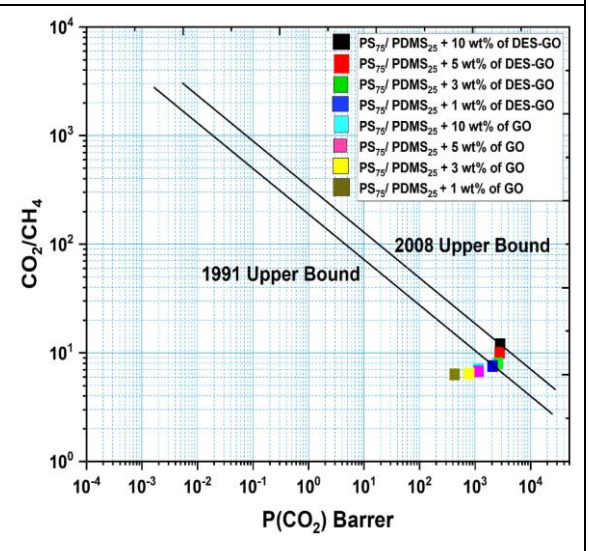

(VI) Robeson upper bound for CO_2/CH_4

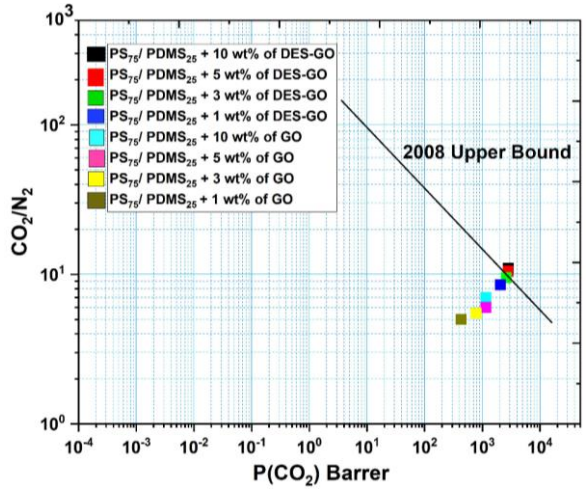

(VII) Robeson upper bound for CO_2/N_2

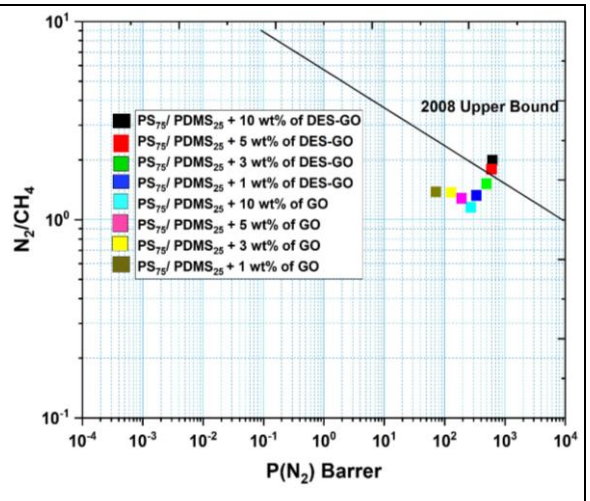

(VIII) Robeson upper bound for N_2/CH_4

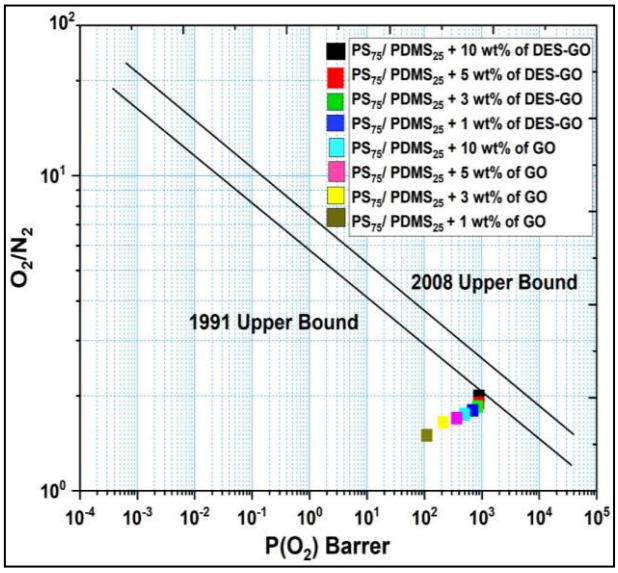

(VIII) Robeson upper bound for O_2/N_2

Figure 5.2.4: Diffusivity Selectivity, Solubility Selectivity and Robeson Plot of different PS/PDMS blends and PS/PDMS - CNT blend composites membranes with respect to different gas pairs ratios

As the DES/GO weight fraction is increases, CO_2 transport becomes faster as more vacancies become accessible for CO_2 molecules. As GO nanofillers contain surface functional groups, varying orientation of fillers and a high aspect ratio, it modifies CO_2/N_2 selectivity. Even, due to the interplay within -COOH and -OH polar groups on GO, the membrane exhibits stronger CO_2 adsorption ability than that of pristine membrane [7]. Therefore, these composite membranes give higher H_2 separation with CH_4 [6]. Usually, for a single gas permeability H_2/CO_2 selectivity is a molecular sieving mechanism as CO_2 gas molecules are strongly absorbed on GO nanofillers [7]. In this experiment, DES modified membrane results in an immense separation performance that is applicable to oxygen enrichment, gasification, natural

gas purification as well as oxy-fuel combustion process. In such processes, it becomes a prerequisite to separate O_2 from the N_2 or other air products.

5.2.3.5 Fourier Transform Infrared (FT-IR) Spectroscopy

Figure 5.2.5 presents the FT-IR spectra of $PS_{75}/PDMS_{25}$ composites with different wt% of GO nanofillers, and $PS_{75}/PDMS_{25}$ composites with different wt% of DES/GO. Figure 5.2.5, the FT-IR spectra of GO shows the peaks, including -OH (3037 cm^{-1}), $-CH_2$ (2923 cm^{-1}), C=O (1725 cm^{-1}), C=C (1928 cm^{-1}), and C-O (754 cm^{-1}), which correspond to the presence of hydroxyl, carboxyl, and epoxide groups on the surface of GO, respectively. The FT-IR spectra of GO and DES/GO nanofillers dispersed in PS/PDMS mixtures showed the appearance of three additional intense peaks. Si-O-Si- (asymmetric vibration at 1026 cm^{-1} and bending vibration at 902 cm^{-1}) and Si-O-C (asymmetric vibration at 1145 cm^{-1} and bending vibration at 685 cm^{-1}) are a pair of instances. These all confirm to the silicon of PDMS presence on the GO surface. The presence of an intensive peak at 1026 cm^{-1} that is associated with the -Si-O-Si bond in all samples indicates that silane precursors present in PDMS have significantly self-condensed, resulting in silicon clusters on the GO surface.

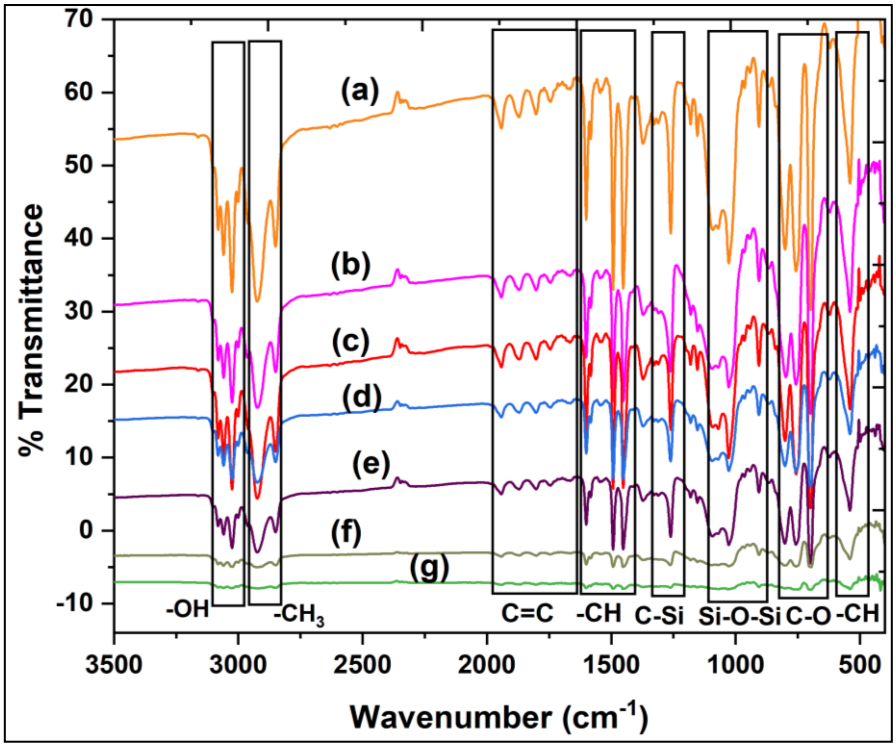

Figure 5.2.5: FT-IR analysis of polymer blend composite membrane and here (a) $PS_{75}/PDMS_{25}$ + 1 wt% of GO, (b) $PS_{75}/PDMS_{25}$+ 3 wt% of GO, (c) $PS_{75}/PDMS_{25}$ + 5 wt% of GO, (d) $PS_{75}/PDMS_{25}$ + 10 wt% of GO, (e) $PS_{75}/PDMS_{25}$ + 1 wt% of DES/GO, (f) $PS_{75}/PDMS_{25}$ + 5 wt% of DES/GO, (g) $PS_{75}/PDMS_{25}$ + 10 wt% of DES/GO

Additionally, by combining with carboxylic groups, the Si-O-C bond confirms the chemical deposition of silicon onto the GO surface. Furthermore, a peak of C-Si was observed at 1264 cm^{-1}, showing that PDMS was attached to the GO surface. Results show disappearance of the carboxyl and epoxide groups of the GO located at 1721 cm^{-1}, 1346 cm^{-1}, and 1264 cm^{-1} indicating the reaction of silicon with the GO surface [9]. These confirm the more silicon group's reaction with the GO surface in the PS/PDMS-GO blend composite and form nanocomposite membrane. The band at 3037 cm^{-1} shows the O–H stretching vibrations of hydroxyl groups. The bands at 1490 cm^{-1}, 1443 cm^{-1}, 520 cm^{-1} and 668 cm^{-1} correspond with –CH and C–O stretching vibrations, C=C vibrations from sp^2 graphitic domains, and C–OH stretching vibrations of carboxylic acid groups, respectively. The FT-IR spectrum shows characteristic bands, which are at 1026 cm^{-1} and 902 cm^{-1} (Si-O-Si stretching from PDMS), 2923 cm^{-1} and 2854 cm^{-1} (–CH_3 symmetric stretching), 520 cm^{-1} and 1443 cm^{-1} (asymmetric and symmetric stretching of -CH), 1864 cm^{-1} and 1930 cm^{-1} (C–C stretching of the aliphatic carbon from DES/GO), 1260 cm^{-1} and (from C-OH bending from DES/GO), 2924 cm^{-1} and 2997 cm^{-1} corresponding to C–H, from CH_3 and CH_2 stretching bands from DES/GO, which also are overlapped with -OH stretching bands in this region.

To show these modifications by GO nanofillers and its functional groups through DES functionalization, we have produced schematics in Figure 5.2.5 which show the chemical structures of GO, and DES/GO. A typical broadband between 3025 cm^{-1} and 3000 cm^{-1} for O-H stretching vibrations. The C-O stretching bands from carboxylic acid groups were only slightly shifted from 754 cm^{-1} in GO to 668 cm^{-1} in DES/GO, however the C=C vibrations for the unoxidized graphene oxide domains at 1928 cm^{-1} to 1698 cm^{-1} were attenuated. Similar to this, the O-H stretching vibration for the GO, which was previously at 3025 cm^{-1}, was reduced following DES functionalization and shifted to 3000 cm^{-1}. In the DES/GO nanofillers, the C=O and O-H bands have shifted, which is an indication that DES functionalization has only partially reduced their intensity [10]. The results of this study showed that there was not only a physical interaction between PS/PDMS and DES/GO, but also a chemical crosslinking. In order to significantly increase the interface contact between polymer and nanofillers in blend composite membranes, modified GO with functionalize DES. The primary characteristic peaks for the DES/GO sample were in concordance with the Si and GO shown in the Figure 5.2.5, respectively. It proves that the PS/PDMS - DES/GO sample is composed of DES and GO with nano-hybrid structure.

5.2.3.6 Differential Scanning Calorimeter (DSC)

It has been observed that the glass transition temperatures (T_g) of blend composites is between 94.24 °C to 96.27 °C, as observed in Figure 5.2.6. A considerable increase in the glass transition temperature of $PS_{75}/PDMS_{25}$ with DES/GO nanofillers blend composites membrane was observed and it is found that $PS_{75}/PDMS_{25}$ with 10 wt% of DES/GO nanofillers membrane has significantly higher T_g than that of other composite membranes and also higher than that of the $PS_{75}/PDMS_{25}$ blend membrane. This might be due to GO's monocrystalline structure, which makes it more difficult to break the bonds between its molecules. Also, after being functionalized with DES, GO became more thermally stable. According to FE-SEM and FT-IR results, the uniform dispersion of GO with DES solvent is the reason for the improved thermal stability of $PS_{75}/PDMS_{25}$ + DES/GO. $PS_{75}/PDMS_{25}$ with 10 wt% of DES/GO fillers have a glass transition temperature that is 96.27 °C, higher than $PS_{75}/PDMS_{25}$ + GO.

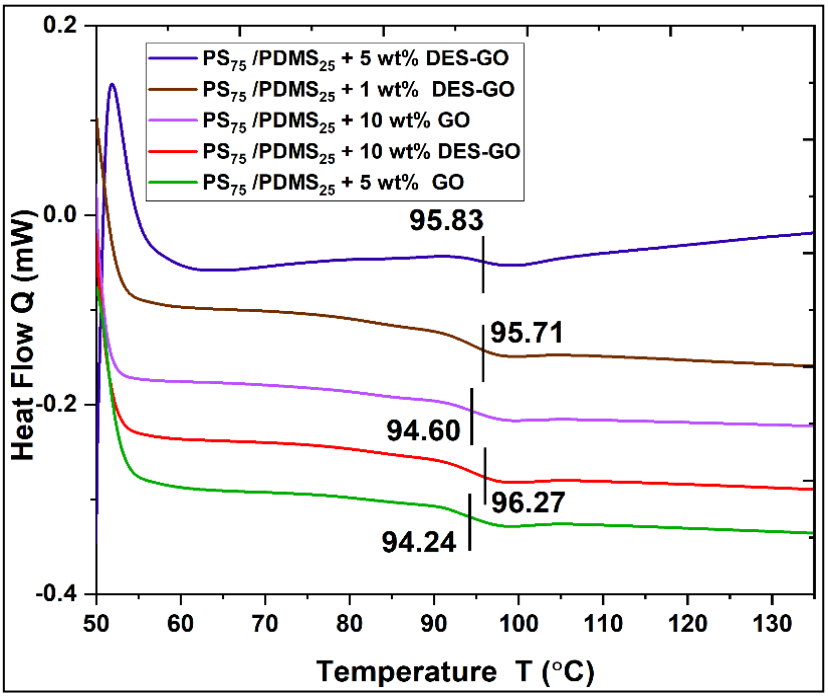

Figure 5.2.6: Shows the DSC thermal analysis of $PS_{75}/PDMS_{25}$ blends with GO and DES/GO nanofillers with different weight ratios of nanofillers

This shows the majority of the GO fillers were covered by the DES solvent layer after being functionalized with DES, which supports lowering of T_g value of $PS_{75}/PDMS_{25}$ with GO glass transition temperature is lower than the $PS_{75}/PDMS_{25}$ + DES/GO glass transition temperature [11]. It also supports another very strong evidence that the composite DES played a crucial role in uniform distribution DES/GO in polymer blends of PNCs.

5.2.3.7 Thermogravimetric Analyzer (TGA)

Thermogravimetric analyzer (TGA) was used to analyze resistance of the membranes to temperature changes as shown in Figure 5.2.7.

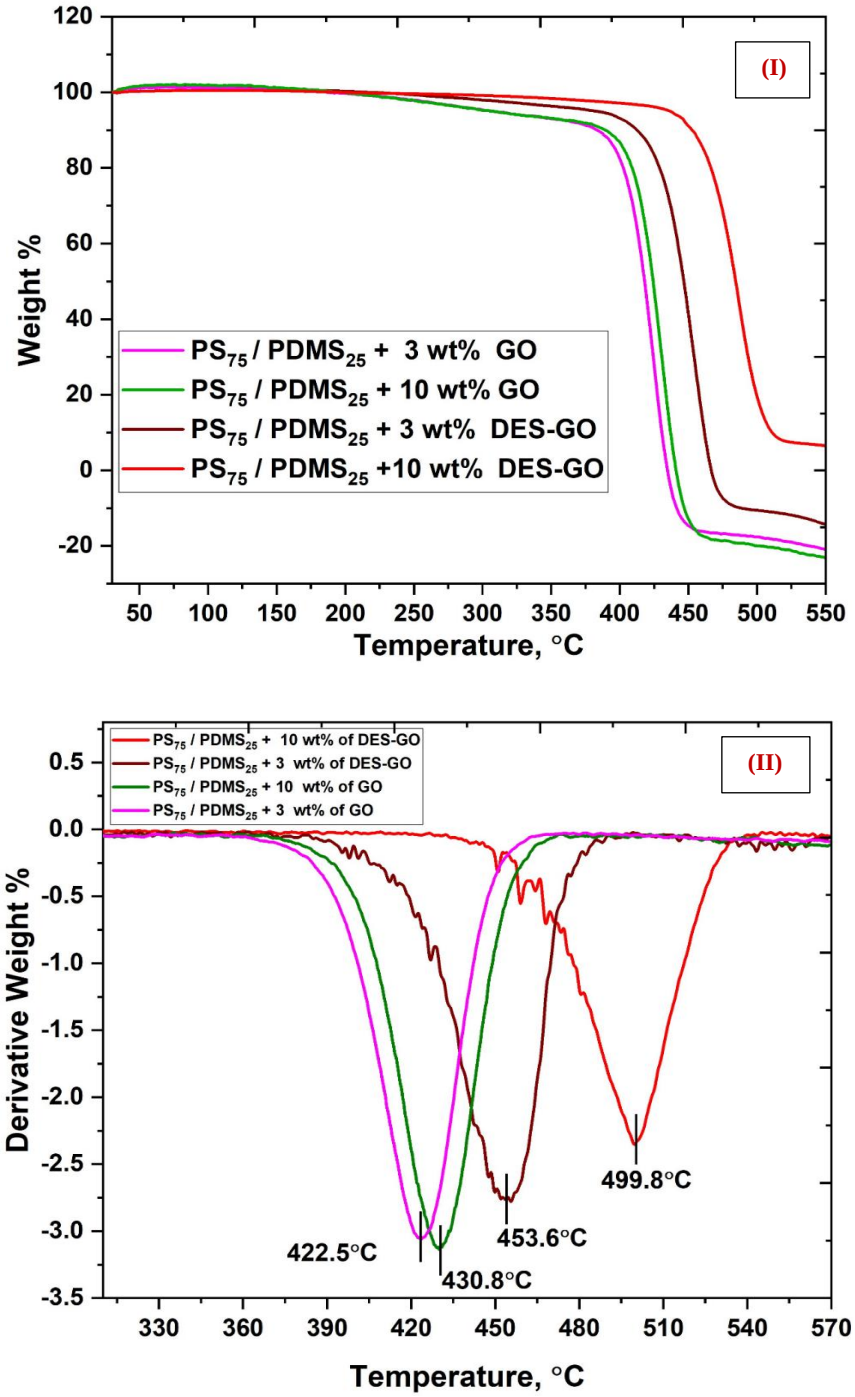

Figure 5.2.7: (I) TGA thermogram and (II) Derivative of TGA thermogram of PS_{75} /$PDMS_{25}$ + 3 wt% of GO, PS_{75} /$PDMS_{25}$ + 10 wt% of GO, PS_{75} /$PDMS_{25}$ + 3 wt% of DES/GO, PS_{75} /$PDMS_{25}$ + 10 wt% of DES/GO

Since PDMS is a type of copolymer containing silica groups (such as siloxane linkages), which might decrease the heat stability, PS/PDMS blends loses the most weight

(95%), and similar observation have been reported in literature [12]. PS/PDMS blends with the higher amount of GO nanofillers lost less weight than that of other nanocomposite membranes, showing that the GO and DES/GO nanofillers significantly improves the heat stability of the PS/PDMS blend composite membranes [13].

The TGA curve of $PS_{75}/PDMS_{25}$ + (GO, DES/GO) shows two phases of weight loss; at 222 °C to 378 °C, this weight loss is due to the evaporation of low-molecular-weight impurities and residual solvent. Weight loss occurs after 378 °C to 520 °C is due to polymer chain disintegration. The depolymerization of nanofillers (GO, DES/GO) in PS/PDMS caused a stage of weight loss in the blend composite membranes between 390 °C and 520 °C. The membrane that has the highest concentration of DES/GO in the $PS_{75}/PDMS_{25}$ blend composition has lowest weight loss and the highest weight loss of $PS_{75}/PDMS_{25}$ + 3wt% of GO. The thermochemical properties of the GO has significantly altered by the composite of modified GO with DES to the PS/PDMS blend membranes. The synthesized membranes based on composite with DES/GO were show thermally stable over a wide range of temperatures [14]. The results show that the temperature of maximal thermal degradation would decrease after fictionalize DES with the increased the amount of DES/GO nanofillers. TGA and derivative thermogravimetry (DTG) of these blend composites membranes thermograms are shown in Figure 5.2.7 (II).

The synthesized blend composites membranes were heated at a rate of 10 °C/min in a nitrogen atmosphere while being studied using TGA which is observed in Figure 5.2.7 (I). Table 5.2.2 provides overview of the breakdown temperatures for various percent weight losses. The temperature of weight losses of 5%, 50%, 95% and T_{max}. The char yield (%) at 500 °C have been studied to determine the impact of composites addition on the thermal stability of $PS_{75}/PDMS_{25}$ blends. Table. 5.2.2 shows different steps of temperature of weight loss steps for all composites at 50 °C - 383 °C (5%), 383 °C - 401 °C (50%), 401 °C - 412 °C (95%) and 412 °C - 499 °C is maximum temperature for weight loss. Decomposition of oxygen-containing groups existed on the GO surface (i.e. hydroxyl, carboxylic and epoxide groups), and decomposition of the carbon skeleton of GO. When compared to all the composites temperatures at which 50% of weight loss has occurred (T_{50}%), the $PS_{75}/PDMS_{25}$+ 3 wt% of GO composites have maximum weight loss and $PS_{75}/PDMS_{25}$ + 10 wt% of DES/GO have minimum weight loss as compared to all other composites [15].

Table 5.2.2: TGA analysis of thermal decomposition of PS/PDMS blends composites with different wt% of GO and DES/GO

Polymer Blend Composites	Temperature at 5%, 50% and 95% of weight loss				Char yield (%) 500 °C
	$T_{5\%}$ (°C)	$T_{10\%}$ (°C)	$T_{50\%}$ (°C)	T_{max} (°C)	
$PS_{75}/PDMS_{25}$ +10 wt% of DES/GO	383	401.45	432.90	499.8	10.2
$PS_{75}/PDMS_{25}$ + 3 wt% of DES/GO	365.45	397.69	415.85	453.6	7.8
$PS_{75}/PDMS_{25}$ + 10 wt% of GO	355.45	388.45	411.38	430.8	2.8
$PS_{75}/PDMS_{25}$ + 3 wt% of GO	346.26	379.62	408.10	422.5	1.6

Decomposition Temperature (Td_{max}) was used to determine the thermal stability. Td_{max} values for blend composite membranes have been obtained to range from 422.5 °C to 499.8 °C, which is observed in Figure 5.2.7 (II). As a result, the thermal stability of $PS_{75}/PDMS_{25}$ blend membranes could certainly be improved by the suitable addition of DES/GO fillers. The results show that the fictionalize GO nanofillers with DES causes blend composites of $PS_{75}/PDMS_{25}$ - DES/GO show less weight loss and to give good thermal stability than of blends of $PS_{75}/PDMS_{25}$ and blends composites of $PS_{75}/PDMS_{25}$ - GO. The value of char yield (%) at 500 °C for 10 wt% of DES/GO is 10.2%, DES/GO (3 wt%) is 7.8%, GO (10 wt%) is 2.8 % and GO (3 wt%) is 1.6%. As a result, the addition of DES/GO nanofillers slows the weight rate and improves the of polymer blend thermal stability, producing a high char yield at higher temperatures [16].

The friction and wear performance test showed that the friction coefficient can be reduced by 27.7% at most, which demonstrates that phenolic resin modified by DES/GO can bear more friction and wear. The results indicate that DES/GO nanofillers show lower weight loss values at 50 °C - 390 °C (5%) than pure GO. The chemical reaction of Si particles of PDMS and DES with carboxylic and epoxide groups in GO increased their decomposition temperature. Lower weight loss values at the end of 700 °C for the DES/GO sample functionalized by DES solvent that higher thermal resistance enhancement of GO when a higher amount of DES covered its surface.

5.2.3.8 Mechanical Properties

A GO and DES/GO nanoparticles composites with the $PS_{75}/PDMS_{25}$ blend may strengthen the tensile strength of materials, elongation modulus, flexural strength and impact strength, which improves by 48.7%, 89.2%, 31.7% and 87.8% at maximum, respectively, the data are shown in Figure 5.2.8.

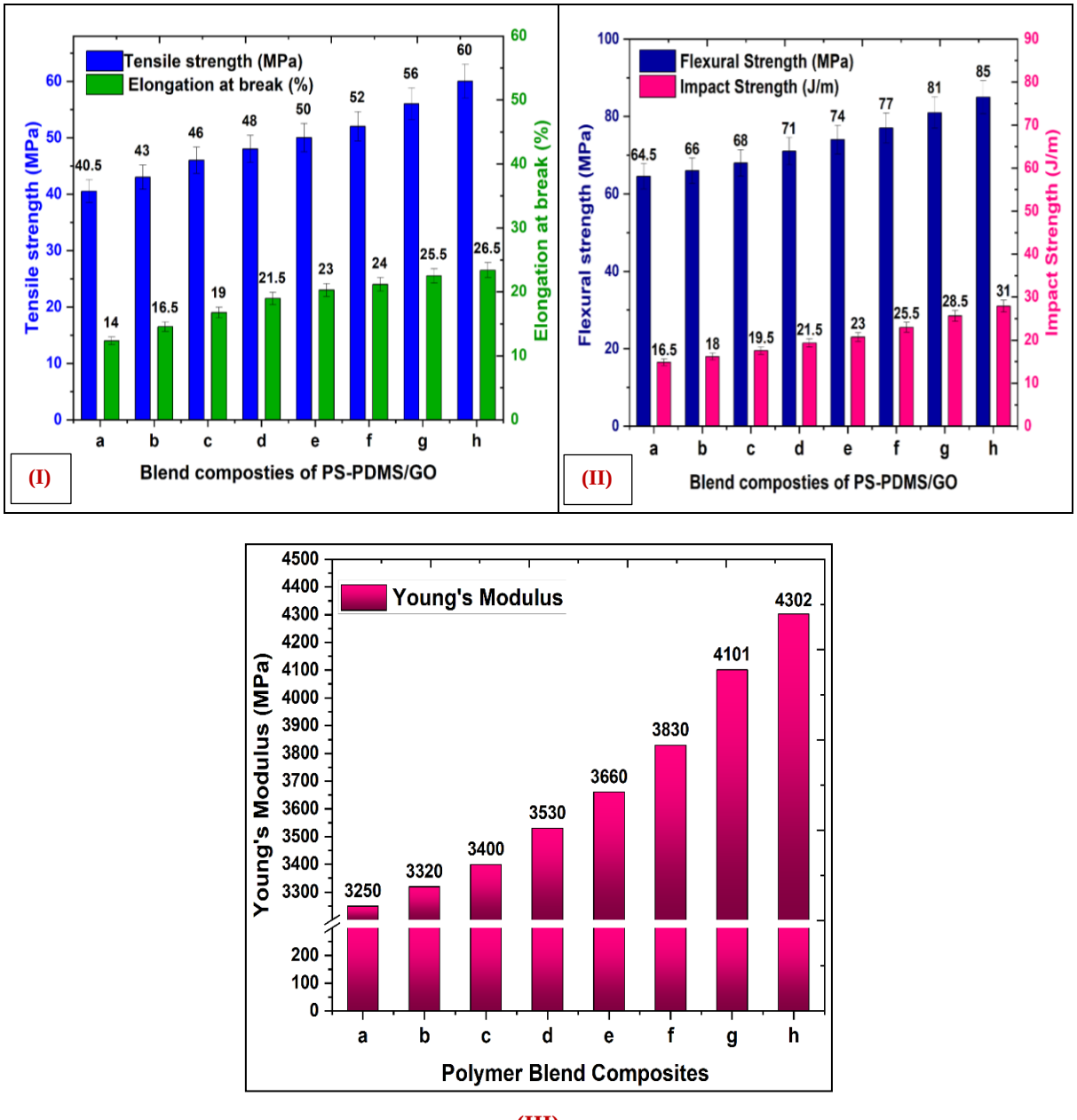

Figure 5.2.8: (I) Tensile strength and Elongation at break, and (II) Flexural strength and Impact strength (III) Young's Modulus of (a) $PS_{75}/PDMS_{25}$ + 1 wt% of GO, (b) $PS_{75}/PDMS_{25}$ + 3 wt% of GO, (c) $PS_{75}/PDMS_{25}$ + 5 wt% of GO, (d) $PS_{75}/PDMS_{25}$ + 10 wt% of GO, (e) $PS_{75}/PDMS_{25}$ + 1 wt% of DES/GO, (f) $PS_{75}/PDMS_{25}$ + 3 wt% of DES/GO, (g) $PS_{75}/PDMS_{25}$ + 5 wt% of DES/GO, (h) $PS_{75}/PDMS_{25}$ + 10 wt% of DES/GO

It has been found that, the DES/GO showed a greater tensile strength and flexural strength than the blend $PS_{75}/PDMS_{25}$, blend composite of $PS_{75}/PDMS_{25}$ + GO. The interaction between hybrid particles of DES/GO composite with $PS_{75}/PDMS_{25}$ blends on a physical and chemical level considerably increased the mechanical toughness of membranes; the similar data are reported [17]. In comparison to blend composites of $PS_{75}/PDMS_{25}$ + GO polymer, the tensile strength for $PS_{75}/PDMS_{25}$ + DES/GO membrane improves and with increasing wt% of DES/GO nanofillers. The cross-section progressively increases with increasing wt% of DES/GO due to many interactions between DES/GO and PS, PDMS. The DES/GO act as a crosslinking site to connect with the polymeric chain in the composites membrane, increasing stiffness. However, when the amount of hybrid particles in the composites increased from 1 wt% to 10 wt%, their strength starts to increase. The highest tensile strength is 60 MPa, the highest flexural strength is 85 MPa and highest impact strength is 31 J/m, significant gains in strain and toughness were found in case of DES/GO, as shown in Figure 5.2.8 (II). For DES/GO, it is found that highest tensile strength as compared the composite with GO nanofillers, the DES/GO composites has higher Young's modulus, it is shown in Figure 5.2.8 (III). The Young's modulus of GO (1 wt%) is 3250 MPa, it increases with increasing the wt% of GO fillers and the highest value of Young's modulus was found to be 3830 MPa for composite with 10 wt% of DES/GO nanofillers [18]. This might be because of the strong molecules interaction between DES and GO. It has been also found, the flexural strength of composite of DES/GO was dramatically increased from 64.5 MPa to 85 MPa. The resulting membranes $PS_{75}/PDMS_{25}$ + DES/GO showed elastic performance with a fracture elongation and Young's modulus respectively, after increasing the DES/GO content from 1 wt% to 10 wt%. This DES/GO composite, which may form more interfacial bonds with the polymer chain-end groups of $PS_{75}/PDMS_{25}$, may the cause of the improved the tensile strength from 40 MPa to 60 MPa, as observed from Figure 5.2.8 (I). Chain mobility has increased by this crosslinking and the tensile strength started to increase at 50 MPa because of increased of this crosslinking of DES/GO composite with $PS_{75}/PDMS_{25}$ blends it provides more strength to $PS_{75}/PDMS_{25}$ + DES/GO blend composites membranes. Figure 5.2.8 (III) shows Young's modulus of the PNCs membranes. The DES/GO composites membranes have greater Young's modulus values than the others composites membranes of GO which has a lower Young's modulus. The Young's modulus of 10 wt% of DES/GO at ideal preparation circumstances was 4302 MPa, or 18% more than that of the GO composite membrane. The results of the studies were carried out on GO composites membranes synthesized in DES solvent provided the greatest improvement of the mechanical characteristics [19].

5.2.3.9 FE-SEM Morphology and EDX

High resolution FE-SEM analysis was used to analyzed the surface morphology of both pure GO nanofillers and DES/GO composites with PS/PDMS blend. Figure 5.2.9 shows SEM imaging and EDX spectra of $PS_{75}/PDMS_{25}$ + GO and $PS_{75}/PDMS_{25}$ + DES/GO membranes shows physical morphology, surface structure and element contain. After DES functionalization, nanofillers show multilayered stacked structures as seen in darker shades for DES/GO compared to light-shaded GO [20]. In Figure 5.2.9, the FE-SEM micrographs of the GO and DES/GO are compared. Figure 5.2.9 (i) shows bulky agglomerates of GO nanofillers (with layered structures at the edges) before functionalized with DES.

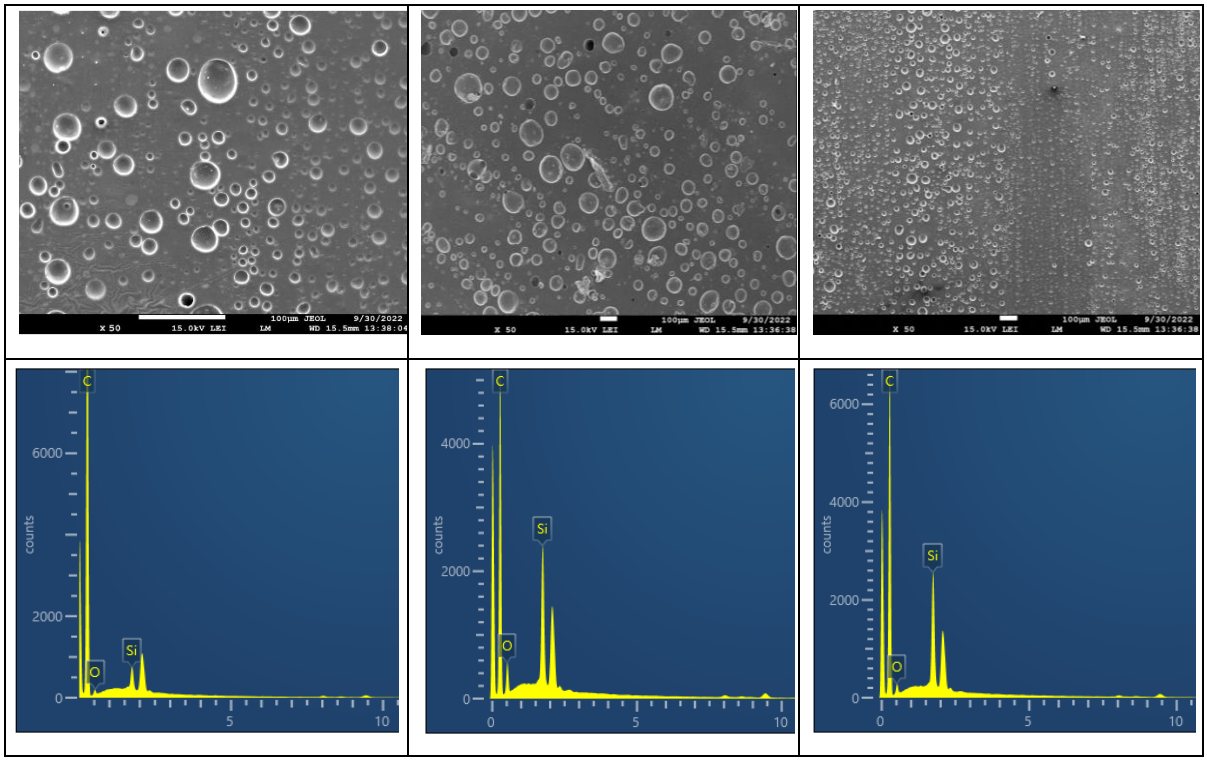

Figure 5.2.9: SEM-EDX analysis of (I) $PS_{75}/PDMS_{25}$ + 10 wt% of GO, (II) $PS_{75}/PDMS_{25}$ + 5 wt% of DES/GO, (III) $PS_{75}/PDMS_{25}$ + 10 wt% of DES/GO

The nanofillers s of GO and DES/GO, on the other hand, showed a puffy shape throughout the functionalization process, suggesting that silicon particles in the PDMS polymer had a role in preventing the re-stacking of GO nanofillers. Based on these explanations the pure GO nanofillers successfully covered with DES. More folding and wrinkling were added to the GO nanofillers when the DES functionalization period was increased from 1 hr to 2 hr; this may be because of the interaction between the functional groups in DES and GO. After

functionalization of GO with DES, that color of the membrane changes to grey and dark grey, respectively, for GO only it is light black when the minimum loading was 10 wt%. The decrease and substitution of the oxygen-containing groups in the GO with other groups is what has caused this color shift [21]. The colors of the GO and DES/GO nanofillers change from light to darker shades as loading increases. The GO and DES/GO nanofillers were uniformly dispersed on the PS/PDMS blend surface by an ultrasonic method since the lateral size of the PS and PDMS polymer is significantly greater than the pore size of the GO and DES/GO nanofillers. Figure 5.2.9 show the composite structure of the synthesized blend composite membranes, which consists of a thin active layer of GO or DES/GO with different wt% of nanofillers has a thickness of ~80 µm on top of a polymeric substrate layer with multiple microvoids. When there is a higher loading ratio of GO nanofillers in the PS/PDMS blends, GO particles produce considerable aggregation parts. Therefore, their capacity for agglomeration was enhanced by increasing the GO concentration.

In Figure 5.2.9, thick polymer blend composite membranes have represented by a smooth surface. EDX analysis was also performed on the GO and DES/GO to obtain amount of element present in material. The EDX test for composite PS/PDMS - (GO, DES/GO) membranes show a small intensity peak of silica due to the blend with PDMS used during membrane synthesis. The dispersed microsphere of the carbon and silica particle was visible in the PDMS in the blend of PS/PDMS composites with GO nanofillers, as shown in Figure 5.2.9, and their presence was confirmed by the considerable intensity peak of C and Si in the blend composites membranes [22].

Table 5.2.3: Elemental analysis of PS/PDMS blends composites with different wt% of GO and DES/GO by using EDX instrument

Elements	**$PS_{75}/PDMS_{25}$-GO (10 wt%)**	**$PS_{75}/PDMS_{25}$-DES/GO (5 wt%)**	**$PS_{75}/PDMS_{25}$-DES/GO (10 wt%)**
	Weight %	**Weight %**	**Weight %**
O	72.8	73.6	73.2
C	27	26.2	26.6
Si	0.2	0.2	0.2

As the wt% of DES/GO nanofillers increases in PS/PDMS polymer blends the amount of carbon increases and the amount of Si remains constant which in observed form EDX spectra. There are some bigger particles due to the aggregation or overlapping of smaller particles. The analysis indicates that the sample exclusively included O and C particles, confirming its high purity and the lack of other impurities [23]. Figure 5.2.9 presents the EDX spectra and elemental composition of these membranes along with corresponding SEM images of the selected membrane surface. From Table 5.2.3 it is observed that the oxygen content increased from 72.8% in $PS_{75}/PDMS_{25}$-GO (10 wt%) to 73.6% in $PS_{75}/PDMS_{25}$-DES/GO (10 wt%). Furthermore, carbon content decreases from 27% to 26.2%, confirming the partial and progressive decrement of GO in a blend of PS/PDMS. Furthermore, a silica content constant of 0.2% in $PS_{75}/PDMS_{25}$-(GO, DES/GO) composite membrane, due to GO nanofillers overlapping PS/ PDMS polymer blend. The surfaces of 12 wt% of GO membranes are smoother than those of 5 wt% and 10 wt% of DES/GO membranes, as shown in Figure 5.2.9 (II and III), and with increasing weight percentages of DES/GO, the $PS_{75}/PDMS_{25}$ - DES/GO composite membranes become more roughened with wrinkles, which increases the flow of gas molecules [24].

5.2.4 Conclusion

A blend of PS/PDMS composite with GO and DES/GO nanofillers have higher mechanical capacities than that of PS/PDMS blend and pure polymers. The composite of DES/GO with $PS_{75}/PDMS_{25}$ offers stronger tensile, flexural, and impact strengths than other composite with GO [25]. DSC test determines the degree of miscibility by measuring single glass transition temperature. Since industrial membrane operations required high operating pressure and temperature. The composites of PS/PDMS blend with DES/GO nanofillers have been observed by using high magnification FE-SEM micrographs, results show less agglomeration of DES/GO nanofillers [26]. GO stuffing has dramatically improved diffusion of gas species by increasing its weight fraction as it contains active functional groups and tailors nano-channels within the interlayer polymer phase. The separation performance shows the overcome the Robeson plots where the composition crosses the Robeson's 2008 boundary. The performance of the membranes for H_2 separation gains attention towards energy as well as industrial applications. Moreover, the highest selectivity has been obtained for CO_2/CH_4 which is applicable for carbon capturing application. For the vast industrial applications, the trade-off parameters must be linearly lifted up towards the commercial interesting region. Thus, the

integration of various modification techniques may lead the membrane technology for a long-term pilot scale industrial application.

References:

[1] A. K. Patel, N. K. Acharya, Thermally rearranged (TR) HAB-6FDA nanocomposite membranes for hydrogen, *Inter. J. of hydro. Ener.*, **2019**, 12, 112-125.

[2] Y. Sakamoto, K. Nagata, K. Yogo, K. Yamada, Preparation and CO_2 separation properties of amine-modified mesoporous silica membranes, *Micro. and Meso. Mater.*, **2007**, 101, 303–311.

[3] M. Asghari, S. Saadatmandi, M. Afsari, Graphene Oxide and its Derivatives for Gas separation Membranes, *ChemBioEng*, **2021**, 8(2), 1–28.

[4] B. B. Hansen, S. Spittle, B. Chen, et. al., Deep Eutectic Solvents: A Review of Fundamentals and Applications, *Chemical reviews*, **2021**, 121, 1232-1285.

[5] S. Rehman, S. Rafiq, N. Muhammad, et. al., Surface tuning of silica by deep eutectic solvent to synthesize biomass derived based membranes for gas separation to enhance the circular bioeconomy, *Fuel*, **2022**, 31, 122355-78.

[6] H. Zheng, L. Zhu, et. al., Two-dimensional graphene oxide membrane for H_2/CH_4 separation: Insights from molecular dynamics simulations, *Inter. J. of hydro. Ener.*, **2017**, 42, 30653 -30660.

[7] M. Chawla, H. Saulat, M. M. Khan, et. al., Gas membranes for CO_2/CH_4 and CO_2/N_2 separation, *Chem. Engine. and Tech.*, **2020**, 43,184-199.

[8] G. L. Jadav, V. K. Aswal, H. Bhatt, J. C. Chaudhari, Characterization of polydimethylsiloxane pervaporation membranes using small-angle neutron scattering, *J. Membr. Sci.*, **2012**, 415, 624–634.

[9] K. H. Li, D. H. Olson, J. Seidel, T. J. Emge, J. Li, Zeolitic imidazolate frameworks for kinetic separation of propane and propene, *J. Am. Chem. Soc.*, **2009,** 131,10368–10369.

[10] G. Liu, F. Xiangli, W. Wei, S. Liu, W. Jin, Improved performance of PDMS/ceramic composite pervaporation membranes by ZSM-5 homogeneously dispersed in PDMS via a surface graft/coating approach, *Chem. Eng. J.*, **2011**, 174, 495– 510.

[11] L. Starannikova, M. Pilipenko, et. al., Addition type polynorbornene with $Si(CH_3)_3$ side groups: detailed study of gas permeation and thermodynamic properties, *J. Membr. Sci.*, **2008**, 323, 134-143.

[12] G. L. Jadav, V. K. Aswal, P.S. Singh, Preparation of bifunctional poly(dimethylsiloxane) membrane by dual X-linking, *J. Matter. Chem. A.*, **2013**, 1, 4893- 4903.

[13] M. Rezakazemi, K. Shahidi, T. Mohammadi, Sorption properties of hydrogen selective PDMS/Zeolite 4A mixed matrix membrane, *Inter. J. of Hydro. Ener*., **2012**, 37, 14576-14589.

[14] G. Lin, M. Abar, L. M. Vane, Mixedmatrix silicon andfluorosilicon/zeolite 4A membranes for ethanol dehydration by pervaporation, *Sep. Sci. and Techno*., **2013**, 48, 523-536.

[15] D. Bastani, N. Esmaeili, M. Asadollahi, Polymeric mixed matrix membranes containing zeolites as a filler for gas separation applications: A review, *J. of Indus. and Engi. Chem.*, **2013**, 19, 375-393.

[16] T. C. Merkel, B. D. Freeman, R. J. Spontak, Z. He, I. Pinnau, P. Meakin, A.J. Hill, Ultrapermeable, reverse-seletive nanocomposite membranes, *Science*, **2002,** 296, 519- 522.

[17] G. L. Jadav, P.S. Singh, Synthesis ofnovel silica-polyamide nanocomposite membrane with enhanced properties, *J. of Membr. Sci.*, **2009**, 328, 557-567.

[18] D. F. Li, T.S. Chung, R. Wang, Y. Liu. Fabrication of fluoropolyimide/polyethersulfone (PES) dual layer asymmetric hollow fibre membranes for gas separation, *J. Membr. Sci.*, **2002**, 198, 211-223.

[19] A. K. Patel, N. K. Acharya, Thermomechanical and gas transport behavior of silica-doped polymer blend nanocomposites, *Nanomater. and Ener.*, **2021**, 10, 101-110.

[20] J. Shen, Mengchen Zhang, Facile tailoring of the two-dimensional graphene oxide channels for gas separation, *RCS Adv.*, **2016**, 59, 54281-54285.

[21] S. Shujaat Karim, Sarah Farrukh, A comprehensive overview of dual-layer composite membrane for air (O_2/N_2) separation, *Poly. and Poly. Compo.*, **2021**, 29, 1630–1640.

[22] M. Han, S.T. Nam. Thermodynamic and rheological variation in polysulfone solution by PVP and its effect in the preparation of phase inversion membrane, *J. Membr. Sci.*, **2002**, 202, 55–61.

[23] N. Widjojo, T. S. Chung, Thickness and air gap dependence of macrovoid evolution in phase-inversion asymmetric hollow fibre membranes, *Ind. Eng. Chem. Res*. **2006**, 45, 7618-7626.

[24] A. F. Ismail, I. Dunkin, S. L. Gallivan and S. J. Shilton, Production of super selective polysulfone hollow fibre membranes for gas separation. *Polymer*, **1999**, 40, 6499-6506.

[25] A. M. Efimov, V. G. Pogareva and A. V. Shashkin, Water-related bands in the IR absorption spectra of silicate glasses, *J. Non-Cryst. Solids*, **2003**, 93, 332-45.